Politecnico di Torino

Master's Degree in Automotive Engineering
Academic Year 2024/2025
Graduation Session: July 2025

HIGH FIDELITY SIMULATION OF A PROTOTYPE HYDROGEN BURNER CONCEPT

A turbulence and combustion CFD study of a JICF Micromix Hydrogen Combustor

Supervisors:

Stefano d'Ambrosio
Alexander Lautenschläger

Candidate:

Riccardo Venturelli

TABLE OF CONTENTS

1 NOMENCLATURE

1.1 CHEMICAL FORMULAS

- H_2 – Gaseous Hydrogen
- CO – Carbon monoxide
- CO_2 – Carbon oxide
- CH_4 – Methane
- C_3H_8– Propane
- N_2– Gaseous Nitrogen
- O_2 – Gaseous Oxygen
- NO_x– Nitrogen Oxides
- H_2O – Water (vapour)

1.2 ACRONYMS

- EGR = Exhaust Gas Recirculation
- SCR = Selective Catalytic Converter
- JICF = Jet-in-Crossflow
- AGP = Air Guiding Panel
- CFD = Computational Fluid Dynamics
- RANS = Reynolds Averaged Navier Stokes
- RSM = Reynolds Stresses Model
- URANS = Unsteady Reynolds Average Navier Stokes
- DES = Detached Eddies Simulation
- LES = Large Eddies Simulation
- SGS = Sub-Grid Scale
- ED-FR = Eddy Dissipation- Finite Rate
- EDM = Eddy Dissipation Model
- EDC = Eddy Dissipation Concept
- FGM = Flamelet Generated Manifold
- PDF = Probability Density Function

- CMC = Conditional Moment Closure
- RoR = Rate of Reaction
- CFL = Courant-Friedrichs-Lewy number
- IR = Impulse Ratio

1.3 PHISICAL QUANTITIES

- $\lambda = Air - Fuel\ equivalence\ ratio$
- $\rho = \ Density$
- $f_i = External\ force$
- $\tau_{ij} = \ Viscous\ stress\ tensor$
- $\tau_{ij}^{R} = \ Reynolds\ stress\ tensor$
- $\tau_{ij}^{A} = Anisotropic\ part\ of\ the\ Reynolds\ stress\ tensor$
- $\nu_T = Turbulent\ Viscosity\ coefficient$
- $k = \ Turbulent\ kinetic\ energy$
- $\varepsilon = \ Dissipation\ rate\ of\ the\ turbulent\ kinetic\ energy$
- $\omega = \ Specific\ dissipation\ rate\ of\ the\ turbulent\ kinetic\ energy$
- $J_i = Impulse\ at\ the\ fuel\ inlet$
- $P_i = \ Pressure\ at\ the\ fuel\ inlet$
- $v_i = Velocity\ at\ fuel\ inlet$
- $\Delta t = Time\ step\ size$
- $\Delta x = Grid\ refinement\ size$
- $l_0 = Integral\ length\ scale$
- $l = Turbulent\ length\ scale$
- $d_h = Hydraulic\ diameter$
- $rms_i = Root\ mean\ square\ velocity$

2 INTRODUCTION

In the context of the research for greener energy production systems, this Master Thesis will introduce the concepts related to the substitution of natural gases with hydrogen in gas turbine applications, explain the motivations behind this change and report the biggest challenges which can be encountered with this substitution and the various solutions found in the literature.

Particular attention will be given to the study of a Dry Low NO_x Micromix Combustor with a Jet-in-Crossflow injection.

It will then cover the theoretical part related to the turbulence models and combustion models that have been studied in relatable applications. The design model will then be described together with the test-rig configuration; the experimental results obtained will be used for validation against the predictions of the models.

The last part will be the CFD study of the Hydrogen burner concept with a particular effort in the application of various kinds of turbulence and combustion models and the identification of the simulation workflow for each one of them. The different models will be studied and compared in the post processing to better analyse their advantages and limitations.

3 COMBUSTION OF HYDROGEN

3.1 Hydrogen as a green alternative

Nowadays, a lot of effort is being put into transitioning the energy sector and the sectors depending on it towards greener alternatives, the two most famous examples being the continuous investments in renewables energy like solar and wind power and the electrification of the fleet of cars.

Hydrogen is defined in the literature as an energy carrier and not as fuel, because it is not possible to find it in the elementary form in nature, so the gaseous form of hydrogen is usually considered as a possibly convenient form of energy transportation. Hydrogen can be considered as a viable and future-proof alternative to fuels and natural gas because of the simple molecular structure that does not contain carbon, meaning that the combustion of hydrogen results in no emissions of hydrocarbons like CO and CO_2.

The environmental impact of utilizing hydrogen as a fuel derives mainly from the method of production of said fuel: as of today, the majority of the hydrogen is produced by steam reforming, a method also called gasification in which natural gases such as CH4 are decomposed in H_2 and other products rich in carbon, this process obtains what it is usually called “grey hydrogen”.

If a system of carbon capture with after-treatment systems (ATS) is implemented in the production of grey hydrogen, the emissions can be cut from 50% to 90% percent depending on the efficiency of said system and the product in this case would be called “blue hydrogen”.

There are other methods of production which have a less of an impact on the environment such as electrolysis and bio-mass fermentation, but even though they represent an alternative to produce “green hydrogen”, there is still the need to develop the infrastructure that would permit them to make a meaningful contribution to the total amount that is being produced nowadays. So, for now, given the quantity of hydrogen needed to decarbonize the thermo-electric energy sector and the automotive one, the combination of steam reforming and systems of carbon capture are the best bet until new investments are done in this sector.

3.2 Hydrogen as a fuel

As a fuel, Hydrogen has a very extended flammability range (4-75%) and it needs a smaller energy input to combust: that creates both opportunities and problems, because even though it is possible to utilize extremely lean mixtures, there is still a worry about the explosiveness of the fuel in the combustion chamber.

Important differences between traditional fuels, natural gas and hydrogen are related to the energy density and specific energy: while hydrogen has an energy density which is up to three times larger than the others, its low density has as a consequence the fact that the energy stored in a fuel tank at atmospheric pressure would not be enough for any kind of application (Corchero & Montañés, 2005). From this problem derives the need to store hydrogen in pressurized tanks (or in liquid or solid form, depending on the opportunity).

	H_2	CH_4	C_3H_8
Molecular Weight $[g\ /mol]$	2.016	16.04	44.097
Density at NTP [$Kg\ /m^3$]	0.0838	0.6512	1.87
Self-Ignition T $[K]$	845–858	813–905	760–766
Minimum Ignition energy [mJ]	0.02	0.29–0.33	0.26–0.305
Flammability range in Air $[vol\%]$	4–75	5–15	2.1–10
Flammability range $[\lambda]$	0.14–10	0.625–2.5	0.37–1.79
Adiabatic Flame Temperature $[K]$	2318-2400	2158-2226	2198-2267
Lower Heating Value $[MJ/Kg]$	118.8–120.3	50	46.35
Lower Heating Value $[MJ/m^3]$	10.78	35.8	91.21

Table 1- Principal chemical characteristics of hydrogen, methane, and propane (Cecere, Giacomazzi, Di Nardo, & Calchetti, 2023)

The research and development of different combustion technologies with H_2 is a needed step to create the premises for investments that could take advantage of the economy of scale and develop a widespread network of distribution.

3.3 Hydrogen Combustion Technologies

The use of a blending of CH4 and H_2 in a gas turbine has already been studied and the results of such blending highlighted the opportunities given by hydrogen in regard to the reduction of pollutant emissions of hydrocarbons, even though, given the lower density, the reduction is non-linear compared to the percentage in volume of hydrogen (Cecere, Giacomazzi, Di Nardo, & Calchetti, 2023).

In the past studies have proved how current turbine designs can be used with a mixture of natural gas and H_2 without encountering problems in the design, but while there is the advantage of not burning hydrocarbons and their subproducts, when implementing the design of full H_2-run gas turbines, the use of pure H_2 will also lead to some problems if the design of the turbine is not optimized for the new fuel. The main

problems are related to the increase of the flame speed, the reduction of the ignition delay and combustion instabilities.

The natural gas combustors were usually pre-mixed to enhance the mixing and limit the emissions of pollutants and the same designs were also able to handle a sizeable percentage of hydrogen.

The design of the turbines must consider how the self-ignition of a 100% H_2 mixture is considerably more frequent than the mixture of a 100% CH4, so it is important that in the hypothetic pre-mixing phase the time models are set in a way to prevent self-ignition. The flame speed of a pure H_2 mixture is also up to an order of magnitude faster (3 m/s instead of 0.35m/s with $\phi = 1$) than the CH4 one, meaning that appropriate steps in the design of the flow must be taken so that the turbine has no problem with the flashback of the flame.

These two characteristics of the mixture could cause potential instabilities in the pre-mixed combustor and may limit its applicability. Peaks of pressure and temperature could compromise the integrity of the entire structure and increase the production of pollutants if the hydrogen is not uniformly distributed when the start of the reaction occurs.

3.4 Hydrogen Combustion Emissions

When it comes to pollutants, the only ones which represent a real problem for the design of a turbine fuelled by an H_2 mixture are the NO_x. As it can be seen from Table 1, the Adiabatic Flame Temperature of hydrogen is higher than the one of methane, meaning that for similar lambdas, hydrogen would be more susceptible to high emissions of NO_x. The formation of these pollutants has been studied extensively, and at least five different reaction mechanisms that may form NO_x from the combustion of hydrogen and air have been studied:

- Thermal NO
- Prompt NO
- NNH Pathway
- N_2O Pathway
- Fuel NO

The prevalent pathways are the “Thermal NO” and the “NNH Pathway” (Cappelletti, Martelli, Bianchi, & Trifoni, 2014) and this study focuses on the former being the main cause of NO_x pollution in a combustor, and it being comprised of the three subsequent reactions:

$$R1: N_2 + O = NO + N$$

$$R2: N + O_2 = NO + O$$

$$R3: N + OH = NO + H$$

For these reactions to take place there is the need for a high activation energy, while the progress of the reactions is limited by the pressure, the temperature, and the residence time. For exactly these reasons the main requirements of a hydrogen burner would be to have a small residence time at low temperature and pressure, in particular, the NO_x production rate has a quadratic dependence with the temperature and its reduction should be the primary focus.

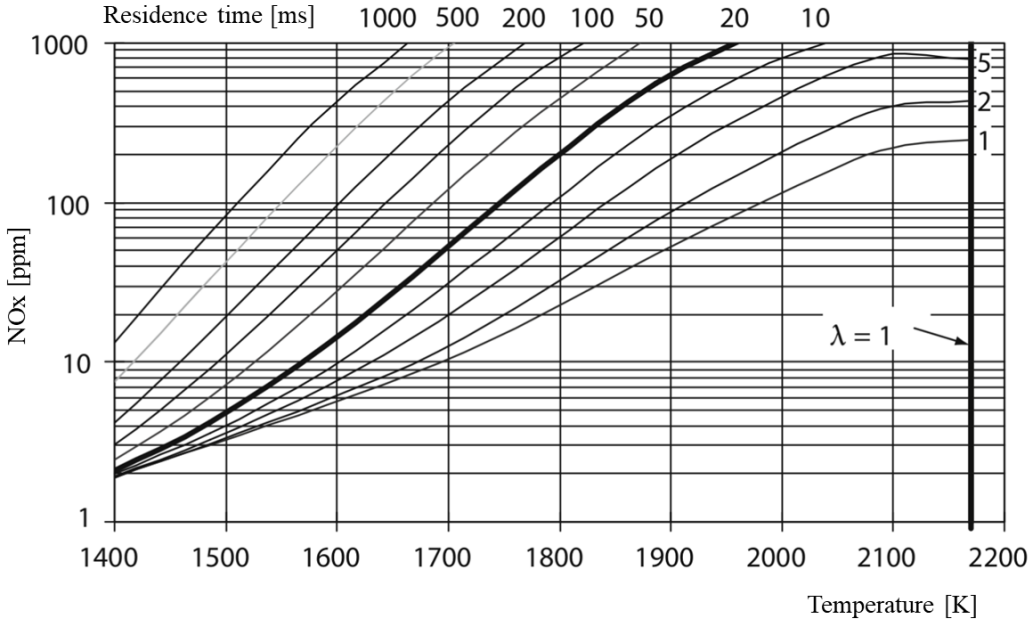

Figure 1 NO_x emissions of a gas turbine for different temperatures and residence times (Ayed A. H., 2017)

The emissions of NO_x can be reduced both actively and passively (also defined as primary and secondary treatment), that means that it is either possible to limit the emission with an updated design geometry which has an inherently lower production in the first place, or the system could be coupled with mechanisms of after-treatment that prevent the release of the pollutants into the environment.

Given that, even though context is needed, the topic of the study is focused on the primary methods of reduction, the secondary methods will be briefly discussed with little interest for the details: two of the most popular methods of passive reduction are EGR and SCR. The first, better known as “Exhaust Gas Recirculation”, consists in introducing again a limited flow of Exhaust gases into the combustor, slowing the reaction rate and limiting the temperature while also reducing the combustion

instabilities. The second one consists in an after-treatment system called “Selective Catalytic Converter” which, also using ammonia as a reactant, can reverse the reaction of NO_x formation exploiting the energy of the hot exhaust gases.

Active methods of reduction focus on design changes in the combustor that would yield better results from the pollutants standpoint, but that implicitly limits the adaptation of actual combustors, given the differences inherent in the design. For this reason, usually only prototypes exist for the possible designs, and a considerable amount of research is still needed before we can see the application of these theories put to practice.

The first big characterization of a new combustor design is the introduction or not of H_2O in the combustion chamber, because, in a similar fashion to EGR, the introduction of water/steam during the combustion would result in lower temperature peaks limiting the NO_x formation. This design choice, as much as it can reduce the NO_x formation thanks to the enhancement of the fuel heat capacity by the water, also has the limit that the presence of H_2O can hinder the combustion of hydrogen, lowering the efficiency of the turbine while also having non-combusted H_2 as an end product.

The choice on the use or not of steam recirculation is the distinction between “Wet Low Emissions” designs (WLE) and “Dry Low Emissions” ones (DLE), being the latter capable of greater efficiencies and of lowering the emissions with a lower level of complexity, this study will focus on the DLE from now on.

When it comes to the combustion design, the main ideas behind Low Emission NO_x Hydrogen combustion technologies can be of different nature and the subsequent list is a non-exhaustive example of the different strategies which have been developed to reduce the NO_x emissions:

- combustion aerodynamically stabilized by propagation;
- combustion stabilized by self-ignition;
- staged combustion, stabilized with different methodologies (by propagation and/or self-ignition);
- micro-mixing combustion, with many small premixed, partially premixed, or diffusive flames.

The idea behind all of this is stabilizing the combustion while avoiding stoichiometric mixture ratio to lower the temperature of the combustion and consequently the production of NO_x.

The concept of the burner that has been considered in this study follows the ideas of the Micromix design, so that will be the next topic of discussion.

3.5 Micromix Combustor

The Micromix combustor is designed so that the combustion is split in a multitude of small flames, every one of which has its own intake ports and injectors (Banihabib, Lingstadt, Wersland, Kutne, & Assadi, 2024). The difference between a conventional burner and a micromix burner is in the fact that a long conventional flame is substituted by many small and short flames, in this way micro mixing aims at limiting the production of pollutants by reducing the residence time (Ayed A. H., 2017), (Funke, Beckmann, Stefan, & Keinz, 2023), (Ayed A. H., Kusterer, Funke, Keinz, & Bohn, 2017).

This design inherently represents a solution to a couple of the problems generated from the use of Hydrogen as fuel: the absence of pre-mixing and direct injection in the combustion flow reduces the problem of self-ignition of the fuel and the chance of flash back, which is problematic in premixed hydrogen-based burners, while the distribution of the mixture through many small flames homogenizes their behaviour and reduces the instabilities in the combustion.

Therefore, the diffusion combustion reduces drastically the chance of flashback, which is related to the velocity of the airflow, but this approach could result in higher peaks of fuel concentration and higher emissions. So, for this reason a particular sub-set of micromix combustors has been developed, and the study will focus on micromix combustors characterized by a Jet-In-Crossflow injection.

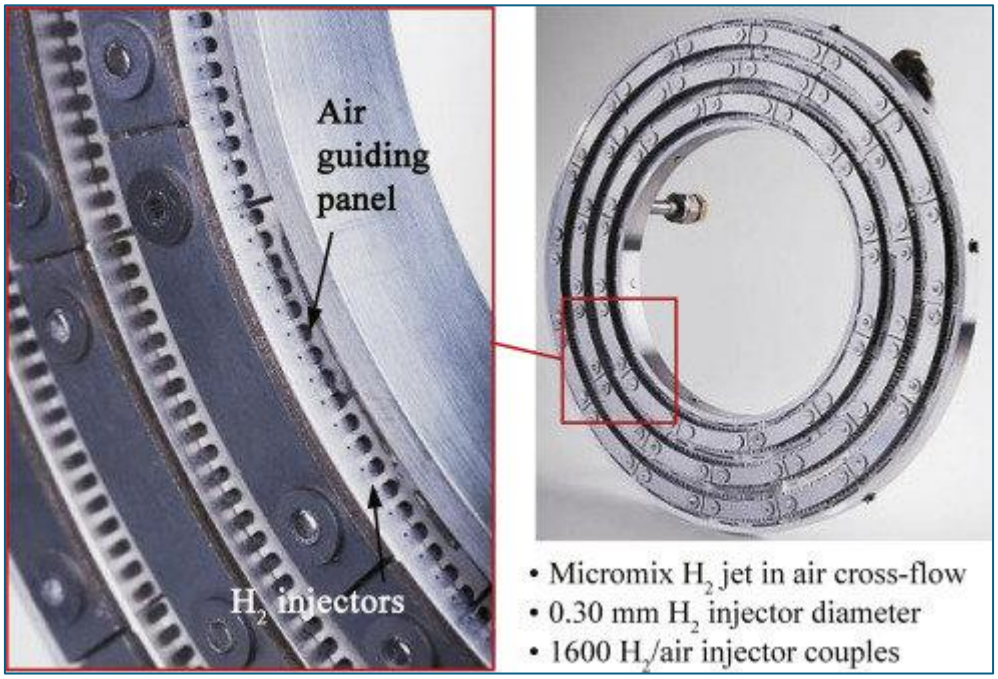

Figure 2 Micromix combustor for gas turbine Honeywell/ Garrett Auxiliary Power Unit APU GTCP 36-300 (prototype)

3.5.1 Jet-in-Crossflow

Jet-In-Crossflow is a particular design of the mechanism of fuel injection in a combustor, and in particular it refers to the injection of the fuel in an incidental direction compared to the stream of compressed air that is driven inside the combustor (New, Lim, & Luo, 2006), (Murugavel, Massey, Tanaka, & Swaminathan, 2024).

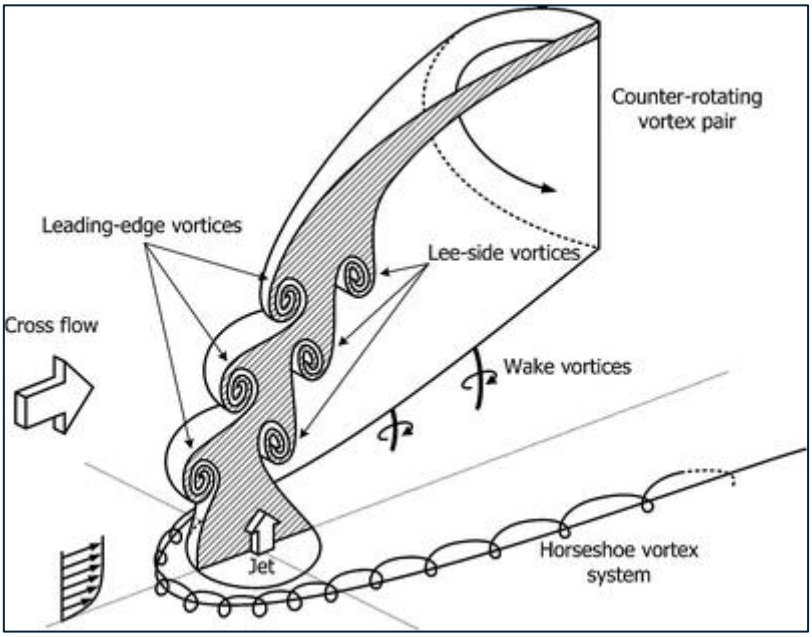

Figure 3 Jet-In-Crossflow representation (New, Lim, & Luo, 2006)

The main advantage of this design is that, especially dealing with Hydrogen, the mixing is enhanced through the multiple small inlets: the small pipes that feed the air speed up the flow and this difference in speed, together with the faster mixing, theoretically reduce the temperatures in the combustor and make it an inherently safer design against flashback.

Furthermore, the rapid interaction between the two perpendicular flow creates various kinds of vortexes which are then responsible for a faster mixing of the charge and shorter flame, all of which being useful to reduce the production of NO_x (Beltran, Sandoval, Llain, Carmona, & Audivet, 2024), (Howarth, Picciani, Richardson, Day, & Aspden, 2024).

Unique designs of Micromix combustors have been developed with this kind of injection in mind, they have in common the presence of a multitude of air nozzles with smaller injectors perpendicular to them. The designs might differ when it comes to shape of the pipes and the dimensions of both pipes and injectors.

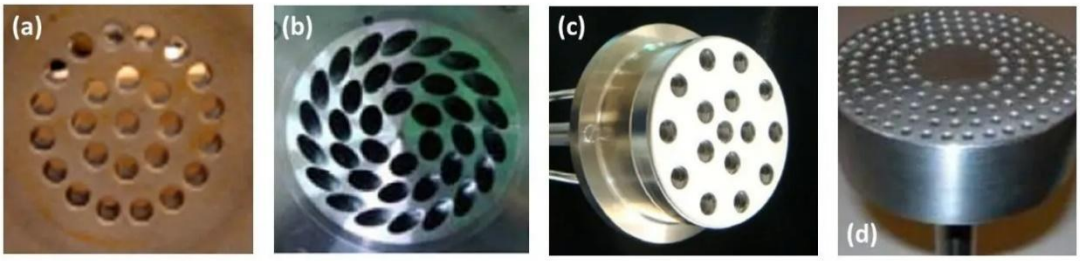

Figure 4 Different prototypes (NASA, Hitachi, Parker Hannifin, and GE Gas Power) (Goldmeer, 2020)

3.5.2 Design of a Micromix Combustor

Figure 5 below represents a section of a micromix burner in which it is possible to identify the air supply, the fuel supply, the air guiding panel, the vortices created by the interaction of all the latter and the flame. We already introduced the concept of the Jet-In-Crossflow, so now the focus will be shifted to the description and use of the Air Guiding Panel (AGP) (Ayed A. H., 2017).

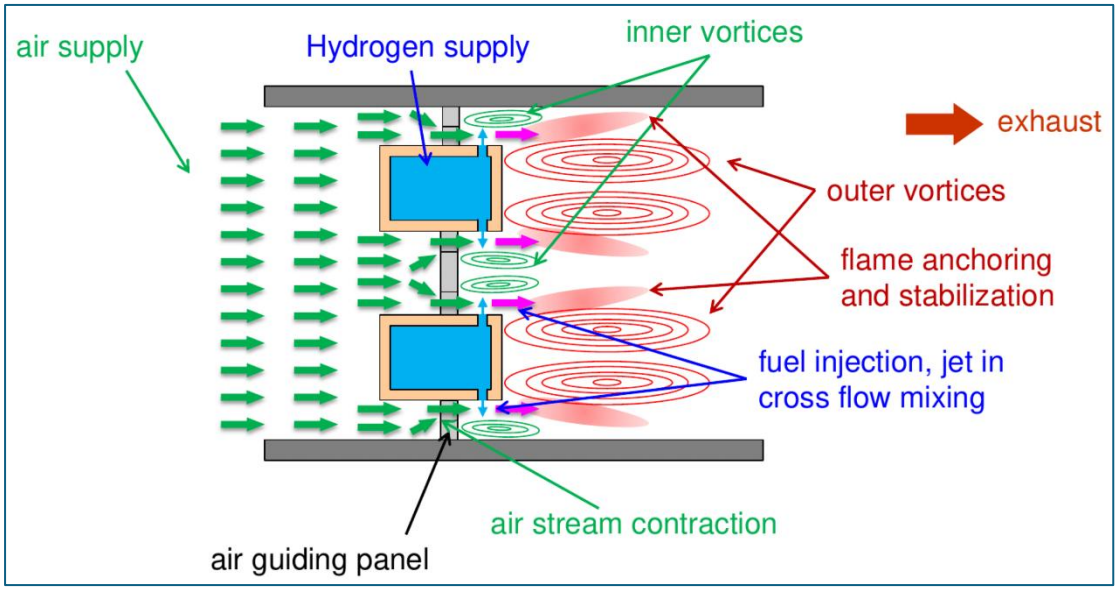

Figure 5 Combustion in a micromix burner

The Air Guiding Panel is an element positioned in the vicinity of the hydrogen injector, while not being co-axial with it. The main idea behind the AGP is that the inflow of air is disturbed by the AGP creating two vortices that help both with the mixing and with the control of the temperature during combustion.

The inner and outer vortices have different dimensions and are positioned asymmetrically one from the other, this is because there is an axial shift between the

AGP and the H_2 injection point, creating an inclined shear-layer between vortices which is where the combustion would ideally take place.

There have been studies on the effect of the dimensions of the AGP on the flow and the combustion (Ayed A. H., 2017), and the main results are that elongating the AGP there is an acceleration of the flow which has as a consequence the elongation of the two vortexes and a rise in temperatures that causes an increased production of NO_x. The smaller the air gap causes higher temperatures in the inner vortex, in which there could be a secondary source of NO_x production. Furthermore, the configuration with the biggest air gap (smallest AGP) has a better performance also in the inter-vortex shear layer because the bigger gap lets colder air pass through and feed the vortexes, lowering the temperature and the NO_x production.

The quantity of hydrogen injected is considered both as an opportunity and a limitation: if the pressure is increased, there is the opportunity to increase the energy density of the burner, but, at the same time, the height of the jet cannot be higher than the air gap of the AGP, otherwise the fuel would feed into the inner vortex, leading to an additional formation of NO_x.

In the study (New, Lim, & Luo, 2006), two different jet velocity profiles were analysed for the fuel inlet: parabolic and tophat profiles, in Figure 6, were compared and the results of the study clearly indicated how the tophat velocity profile had a more suitable behaviour for this kind of application, while the parabolic profile had a bigger penetration capability which hindered the maximum amount of fuel injected before the jet reached the critical height in the channel.

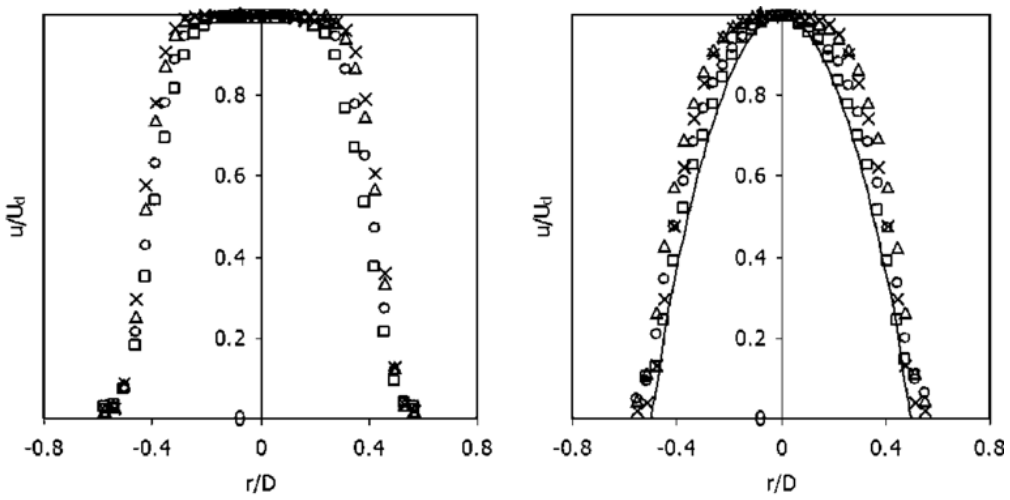

Figure 6 Tophat and Parabolic velocity profiles

It is important to mention, though, that the apparatus needed to create the tophat velocity profile is a lot more complicated and it is easy to imagine how this would not be applicable for a larger number of miniaturized jets.

The dimensioning of the burner, i.e. the dimensions of the injectors, the distance between them, the dimensions of the air pipes and of the AGP is done to obtain the maximum possible energy density while retaining the characteristics of the micromix combustor, this means that one of the key aspects of the design is reducing the distance between injector to fit more while also avoiding flame merging. Flame merging is a phenomenon in which flames interact with each other creating a longer flame and longer residence time in the hot zone for the reactants.

Another limiting factor of the design is the difficulty in the machining process of the small injectors, leading to the analysis of the impact of bigger injectors with a scaled-up distance between injectors (reference). The results highlight that, for larger injectors and a higher energy density, the upscaling of the burners can even result in lower NO_x emissions if the height of the AGP is increased proportionally to the injectors. This is because the higher volume of cold air let in reduces slightly the temperature of the outer vortex and, therefore, also the NO_x production. Another consequence of the higher quantity of fuel injected, that is obviously not by design, is that it is possible for the flame to elongate outside of the region between the two vortices, as shown in Figure 7, in a region characterized by lower air velocity that causes an increase in the residence time of the hot gases.

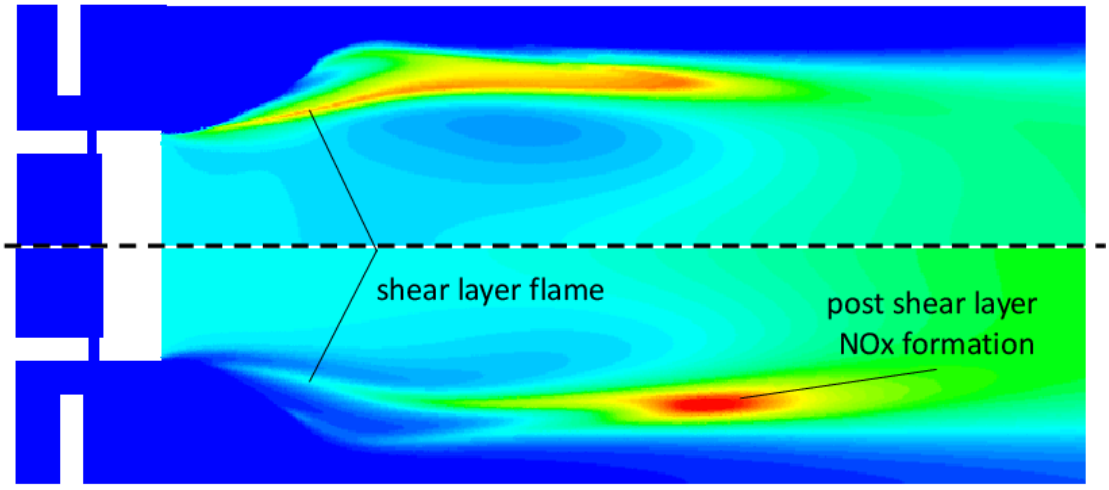

Figure 7 Difference between shear layer and post-shear layer NO_x formation

This phenomenon is defined as combustion in the "Post shear layer", which is located downstream of the vortices, and it is a second flame region not typical for the micromix burning principle, given that the ideal situation would be a complete combustion in the inter-vortex shear layer, where the vortexes can mitigate the surge in temperature and

in so doing also limit the NO_x creation. This phenomenon must be eliminated to support the upscaling of the burners, which is a design objective given that the energy density could get several times higher, while less stringent requirements on the machining process could be applied.

Different design modifications have considered in this regard:

- Variation of the anchoring point from the fuel injector
- Variation of the AGP height
- Variation of mixing geometry

The study conducted on the burner head compared the behaviour of the burner while progressively elongating the burner head to move the anchoring point of the flame further from the injector (Ayed A. H., 2017). The results were that a longer distance between those two points gave more time for the mixing of hydrogen and air, thus avoiding higher concentration of hydrogen, achieving lower temperatures, and lowering the production of NO_x.

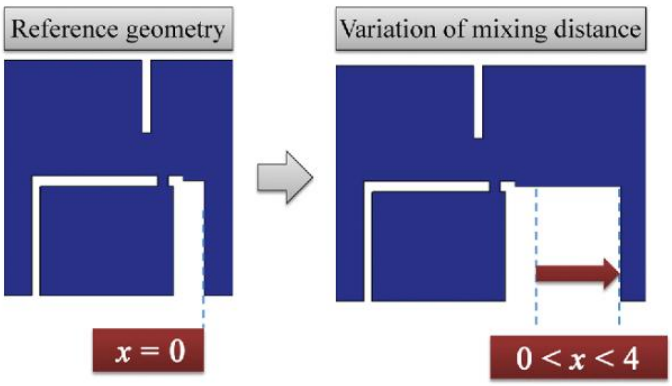

Figure 8 Variation of mixing distance

The Air Gap Panel can also be designed elongated, so that the two symmetric hydrogen burners that face each other are more separated while maintaining the same air gaps. This creates the premises for a longer inner vortex and, by consequence, a longer shear layer between the vortices. The consequence would be an increase in the size of the shear layer and a reduction in the chances of the flame to develop in the post-shear layer.

Therefore, the modification of the burner would be ideal, but it needs to be considered that increase the distance between injectors to create larger vortices also reduces the

power density of the combustor, rendering the whole design less efficient for applications where the volume of the combustor is a limiting factor.

The variation of mixing geometry achieves comparable results starting from analysing and changing the design of a different element of the combustion: the burner head. In particular, the end of the burner head (near the anchoring point of the flame) has been modified creating a stepped pattern.

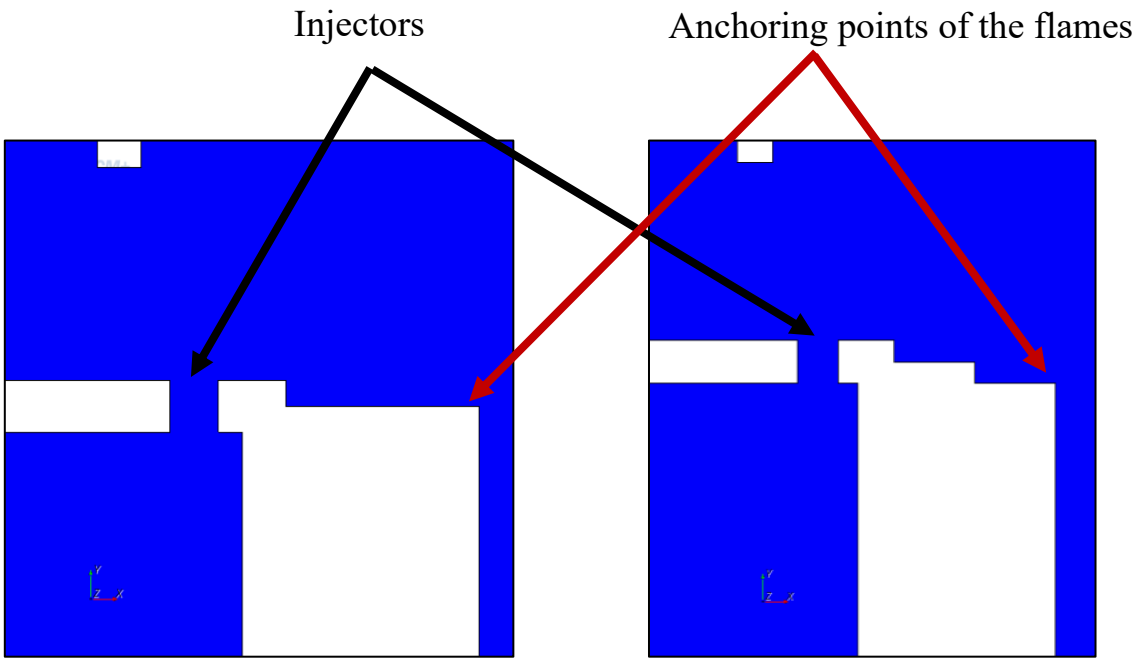

Figure 9 Difference in design of the wall downstream of the hydrogen injector

In this way it essentially pulls both the mixture and the cold air further down, so that the flame develops in a lower region than in the baseline model, enlarging the inner vortex and consequently elongating the shear layer where the flame can develop. This design is also able to sustain longer flames because there is less of a chance of flame-merging, given the extra space that the flame is given to develop.

4 NUMERICAL MODELLING

This part comprises of the theory behind the different models analysed in this study, the models were discussed first with the illustration of the theoretical idea behind them, and then with the description of the physical meanings behind the formulas, when applicable.

4.1 Turbulence Models

The study of fluid dynamics has become an essential part of the design phase of a great part of the industrial products which are nowadays on the market. The advantages are obviously related to the speed at which simulations can be developed, while also reducing the cost of all the necessary equipment that someone would need for a testing rig.

The tool used in this work is Ansys Fluent, a software that is specialized for the meshing and solution of a CFD calculation, CFD being the acronym for Computational Fluid Dynamics.

The CFD simulations are solved thanks to different models that approximate the behaviour of the flow to various extent, the most used ones are the RANS models, while URANS and LES are time-dependent alternative that are considered valid options when the flow has important transient behaviours, but otherwise not considered really suitable because the higher computational cost of these models limits their commercial use.

4.1.1 RANS

The word RANS is an acronym for the title “Reynolds Averaged Navier Stokes” and represent the most popular models used in CFD simulations (Garcia Lovella, Herrera Moya, Jayasuriya, & Blondeau, 2024), (Benim, 2024). If the specific RANS model is chosen correctly, they are considered among the most stable models and that makes them fairly dependable in a lot of situations.

Considering the incompressible, constant density, Navier-Stokes equations

$$\rho\frac{\partial v_i}{\partial t} + \rho\frac{\partial}{\partial x_i}\left(v_i v_j\right) = -\frac{\partial p}{\partial x_i} + \frac{\partial \tau_{ij}}{\partial x_j} + f_i \quad (1)$$

With:

$$\frac{\partial v_i}{\partial x_i} = 0 \quad (2)$$

Where the viscous stress tensor is defined as

$$\tau_{ij} = 2\mu S_{ij} = \mu\left(\frac{\partial v_i}{\partial x_j} + \frac{\partial v_j}{\partial x_i}\right)$$

(3)

and f_i is an external force, we then compute the Reynolds Average of these equations obtaining:

$$\rho\frac{\partial \overline{v}_i}{\partial t} + \rho\frac{\partial}{\partial x_i}\left(\overline{v_i v_j}\right) = -\frac{\partial \overline{p}}{\partial x_i} + \frac{\partial \overline{\tau}_{ij}}{\partial x_j} + \overline{f}_i$$

(4)

The RANS models are operated on the premise that resolving numerically the Navier-Stokes equations for the entire simulation is incredibly difficult both from a computational point of view and a temporal one. For this reason, there has been the need to develop a simplified version of those equations, in which every flow variable is split in a mean and in a fluctuating component, the fluctuating part being considered null. The equations are therefore averaged with different formulas which lead to unclosed terms of the governing equations which we define as Reynolds Stresses.

In Equation (4) there is a non-linear term $\overline{v_i v_j}$ that needs to be resolved, and we need to add the Reynolds Stress Tensor τ_{ij}^R which deals with all the unclosed terms that we obtain with the averaging. The tensor is defined in the isotropic part as:

$$\tau_{ii}^R = -\rho\overline{v_i' v_i'} = -2\rho k$$

(5)

where k is the turbulent kinetic energy. In the meantime, we define the anisotropic part as:

$$\tau_{ij}^A = \tau_{ij}^R - \frac{1}{3}\delta_{ij}\tau_{kk}^R$$

(6)

which usually is modelled using the Boussinesq approximation. Conclusively, by defining:

$$P = \overline{p} - \frac{1}{3}\tau_{kk}^R = \overline{p} + \frac{2}{3}\rho k$$

(7)

we obtain the RANS equation,

$$\rho\frac{\partial \overline{v}_i}{\partial t} + \rho\frac{\partial}{\partial x_i}\left(\overline{v}_i\overline{v}_j\right) = -\frac{\partial P}{\partial x_i} + \frac{\partial \overline{\tau}_{ij}}{\partial x_j} + \frac{\partial \tau_{ij}^A}{\partial x_j} + \overline{f}_i$$

(8)

4.1.1.1 TWO EQUATIONS MODELS

The two most famous models that implement this equation are called "two-equation models", developed with the assumption that the turbulent viscosity coefficient ν_T, which the term that defines the anisotropic stress tensor, is a function of two quantities which are functions of space and time and totally empirical quantities like k, ε and ω, the first being the "turbulent kinetic energy", the second being the "dissipation rate per unit of mass of the kinetic energy" and the third being the "specific dissipation rate".

These equations represent the baseline for a vast variety of models, after having expressed them and having described their formulation, in this study will be further analysed only one case which represents the starting point for the CFD analysis of the burner.

4.1.1.1.1 k-ε model

When using this model, the turbulent viscosity coefficient is set as $\nu_T = \nu_T(k, \varepsilon)$ where $k = \frac{1}{2}\overline{v_i'^2}$, while choosing the ε as

$$\varepsilon = \nu \overline{\frac{\partial v_i'}{\partial x_j}\frac{\partial v_i'}{\partial x_j}}.$$

(9)

Analysing the dimensions of k ,ε and ν_T we can define the turbulent viscosity as

$$\nu_T = C_\mu \frac{k^2}{\varepsilon}$$

(10)

where C_μ is a non-dimensional parameter, usually defined as $C_\mu = 0.09$.

This model has been studied extensively, and it is considered to perform the best in the study of free flows, while showing severe limitations in the near-wall regions. It is not rare, however, to see this model used also in those circumstances if it is developed as a two-zonal model, in which the first one is the k-ε model in the free flow, while the second one is a specific wall function in near-wall conditions.

4.1.1.1.2 k-ω model

The k-ω model is based on the same principles as the k-ε one, but it considers the specific dissipation rate ω instead of ε.

This means that the turbulent viscosity depends on k and a physical quantity ω which has as dimension the inverse of time, meaning it could be either a frequency, r.m.s. of

vorticity fluctuations or the dissipation rate normalized with the turbulent kinetic energy.

To obtain the RANS equation for this case it is possible to express ε in terms of ω and k:

$$\upsilon = \frac{k}{\omega} = C_\mu \frac{k^2}{\varepsilon} \tag{11}$$

And, therefore,

$$\varepsilon = C_\mu k \omega \tag{12}$$

The coefficients appearing in the two-equation models are tuned analysing an ideal flow and they are different for the different models.

The k-ω model usually gives good and stable results when analysing a flow with stringent boundary conditions, as it is more accurate in the near-wall region while having more uncertainties when dealing with free shear flow.

4.1.1.1.3 k-ω SST model

This model is a modified version of the k-ω model, where the acronym stands for Shear Stress Transport, which is coincidentally one of the weaknesses of the base model.

This represents the reference model for the study, and it was developed by Menter in 2003. The idea behind this model is to create a hybrid between k-ω and k-ε so that it would retain the near wall performance of k-ω without being limited in the free shear flow region (Younoussi & Ettaouil, 2024), (Kosiak, Yanovych, Uruba, & Duda, 2024). He achieved it by defining the cross-diffusion term as the k-ε equivalent in k-ω and applying a blending function which, depending on the region of the burner, approximates the cross-diffusion term to k-ω or to the k-ω version of k-ε.

This model is based on the Bradshaw assumption that makes it possible to estimate the shear stress distribution in the boundary layer wake region, as it is considered proportional to the turbulent kinetic energy. This gives the model a better accuracy when dealing with flows with severe pressure gradient flows (Townsend, Xu, & Jin, 2024).

The limitation of this model comes from the use of the same Boussinesq approximation that hinders the accuracy of RANS and misaligns the model predictions when compared to the true Reynolds Stress tensor. The addition of a parameter that contains both the turbulent viscosity and a production term to the approximation seems to achieve the desired results (Rahman, 2023).

Having information on the shear stress tensor makes this model more accurate even far from the boundary conditions, whereas the standard k-ω model is not as dependable in free stream air. This model shows potential also for the study of transient behaviours, where standard RANS would be at a disadvantage.

4.1.1.2 Transition SST model

The transition SST model was developed as the combination of the k-ω SST model and the gamma-Re theta model, also known as transition model (Zhang, Nie, Meng, & Zuo, 2022). This second model is described by other two transport equations which define the Intermittency Factor γ, which is a measure of the probability that a given point is located inside a turbulent region, and the Transition Onset Criteria, defined in terms of the momentum-thickness Reynolds number $Re_{\vartheta t}$ (Yuntao, Yulun, Song, & Dehong, 2015).

The only modification needed to correlate the two sets of equations is the modification of the production and dissipation term in the transport equation of the turbulent kinetic energy.

The transition model is widely regarded as a reliable and fast model given the need to solve only two equations, but also with the combination with the k-ω SST model, the four equations model produces good prediction while being still relatively fast in the computation.

The γ-Re_{ϑ} model has been mainly used in airfoil studies for predicting airflow separation and the onset of turbulence, so, it was questioned whether the Transition SST model could be applicable to our geometry. Eventually the model was included in the study as it seemed like the k-ω SST positively influenced the model to be able to predict highly turbulent behaviour as it was reported in (Benim, 2024).

4.1.1.3 RSM BSL

The Reynolds Stress Model (RSM) is probably the most advanced type of RANS model in which the Boussinesq approximation is abandoned, and the Reynolds Stress Tensor is solved directly with six transport equations and the dissipation equation (Sun, 2023). Of the seven quantities, only four need to be modelled and the two whose approximation limits the accuracy of the model are the pressure/strain term and the dissipation one (Speziale, Sarkar, & Gatski, 1990), (Mishra & Girimaji, 2017).

The transport equations from (Mishra & Girimaji, 2017) have the following structure:

$$\frac{dR_{ij}}{dx} = P_{ij} - \frac{\partial}{\partial x} T_{ijk} + \pi_{ij} - \epsilon_{ij}$$

(13)

Where R_{ij} represents the Reynolds stress tensor, T_{ijk} is the transport term, ϵ_{ij} is the dissipation term and π_{ij} denotes the pressure-strain correlation.

This individual analysis of the Reynolds stresses is considered more useful when the flow is dominated by a strong rotation, since the flow does not obey the isotropic assumption of the Boussinesq approximation.

There are various kinds of RSM models, of which the main ones are RSM BSL and RSM S- ω (Madaliev, et al., 2024). In the RSM BSL (Baseline), the model that will be the focus of our attention, the dissipation term is approximated using the Baseline ω - scale equation, this combination assures a better accuracy in free flow conditions while taking into account the near-wall zone, so that a wall function is not needed.

Studies have shown how the RSM S- ω appears to have greater capabilities in the prediction of vortices and the wall-drag coefficient, while the RSM BSL has a better ability to detect the larger and more pronounced eddies in the flow (Madaliev, et al., 2024), (Long, Tian, Nathan, Chinnici, & Dally, 2015), (Kosiak, Yanovych, Uruba, & Duda, 2024).

Depending on the characteristics of the flow, it could happen that the RSM model, although being a refined version of the RANS one, does not yield improved results and it may be deemed not worthy because of the additional computational costs (Yilmaz, Cam, Tangoz, & Yilmaz, 2017).

4.1.2 URANS

Unsteady RANS models can be useful when dealing with turbulent flows that are time-dependent and exhibit fluctuations even with steady state boundary conditions. As previously implied, the RANS models are not able to deal with transient conditions and, although the turbulent viscosity tensor is still not solved, URANS are the evolution step to correct this defect (Caramia, Amirante, & De Palma, 2024).

The URANS models use a fixed global time step instead of an optimized value for every cell, so if the time step is small enough the URANS are able to capture unsteady and transitional behaviour, rendering them more accurate (Yoder, DeBonis, & Georgiadis, 2013). This solution surely enhances the precision of the predictions, but it is also costlier than a simple RANS model.

URANS, when compared to more accurate model like LES, even though their unsteady behaviour prediction is enhanced, behave similarly to RANS because these models are not able to determine the fluctuations in the flow field velocity, leading to a misrepresentation of the whole part related to turbulent mixing. The URANS model

could be useful when studying periodic or quasi-periodic flows, but they are not suitable when medium-to-small scale eddies are an important part of the flow field development.

4.1.3 LES

LES models (Larger Eddy Simulation) represent a completely different approach to the task of doing CFD simulations, as they aim to directly resolve the largest Eddies, where most of the turbulent energy is, in a direct way without approximations. Intuitively, the higher percentage of turbulent energy is solved directly, the higher the estimated accuracy of the model is (Posch, et al., 2025), (Mehl, Poncet, Truffin, & Colin, 2024).

This means that the largest turbulent behaviour of the flow can be derived accurately, while also taking into account the transient behaviour and the severe pressure gradients encountered. The second part of the simulation would then be resolved with a SGS model (Sub Grid Scale) that approximates and describes the smaller eddies (Smagorinsky, 1963), (Nemati, Ong, & Walther, 2022), (Donepudi, et al., 2024), (Yoder, DeBonis, & Georgiadis, 2013), (Batten, Goldberg, Kang, & Chakravarthy, 2011).

Given how crucial it is to solve accurately the larger eddies in LES simulations, it is important to define the boundary conditions if the inflow is not completely laminar, As the turbulence at the inlets heavily affects the vortices downstream and any variation could cause higher divergence from the solution. This a problem that does not occur when working with RANS, as in that case only the average value of the flow must be provided.

To distinguish between large eddies to be calculated directly and the small eddies to be modelled, there is the need to implement a function to filter them, but the filtering is greatly influenced by the mesh size., so when it is applied to a finer mesh, a finer filter function would make the LES simulation resemble a DNS simulation.

So, even though the LES simulations give better results in general, there is still the need to choose the proper mesh size and time step, as there have been studies that highlighted how choosing a mesh which is too coarse rapidly deteriorates the results of the simulation compared to RANS, this is an important talking point since LES is already a lot more computationally demanding then RANS. Furthermore, it seems like speeding up the simulation by trying to redesign the mesh is much more complicated as well.

In our case of study, studies suggest that a key difference between RANS and LES models would be the underestimation of the mixing in the RANS model compared to the LES ones, given how crucial the mixing is the burner considered, this could represent another counter point against the use of RANS.

4.1.4 HYBRID RANS/LES

One of the computational limitations of LES models is that to obtain correct predictions, the near-wall region must be completely and thoroughly defined, otherwise, if the refinement were not ideal, the near-wall model function would have trouble filtering the eddies and it would deteriorate the whole simulation.

The Hybrid RANS/LES models are of various types, and they exploit a Wall function or RANS model to relax the constraint in the near-wall region, while modelling with LES in the regions away from the walls, especially because the important turbulence for the mixing and the combustion develops in the free stream region (Sa, et al., 2025). This approach has obviously the advantages of having great accuracy in the free stream given by the LES model while the modelled near-wall region significantly reduces the computational costs.

In particular, the DES (Detached Eddy Simulation) model is able to use various RANS models to predict the near-wall flow behaviour and it would be a prime candidate for more in-depth analysis on the optimal amount of large eddies that needs to be solved directly with LES to obtain precise results without weighting the simulation down.

It is possible to choose where the transition zone from to RANS and LES is located by choosing the refinement of the zones of interest and then defining the right time-step size that goes with it.

4.2 Combustion Models

Given that the turbulence models are a tool to analyse the behaviour of the vortices and the mixing, there is still to evaluate how the combustion of the hydrogen can be modelled on the CFD software.

Once the turbulent model has described the flow behaviour, the next step is to develop the combustion of the mixture with particular attention to the temperatures obtained and the relative products formation.

When dealing with combustion, the first phase of the work focuses on the analysis of the Chemical Kinetics, which are the ensemble of all the species and reactions considered in the combustion. There is the possibility to limit the number of species to the minimum, considering only the reactants and products of the combustion with their related reactions, or the list of species can be upgraded to include subproducts and species present in intermediate reactions.

It is obvious that the limitation linked to the simplest model is a likely overestimation of the final products and an underestimation of the incomplete combustion that has as products the intermediate species, in the meantime the most accurate models tend to be computationally costlier while including sub-species which could also not partake in the reactions, therefore slowing the simulation down without a real gain. For this particular application it can be stated without doubt that the concentration of unburned gases at the outlet is negligible, therefore, the simplest model would probably be the best to use.

4.2.1 Chemical Kinetics Models

In this study different ChemKin (Chemical Kinetics) models have been used, when focusing on the turbulent behaviour of the flow at the crossflow the simplest model with only reaction has been used, this choice was made considering that the formation of the thermal NO_x would have been calculated regardless by FLUENT and including those species in the ChemKin would have been redundant.

For the combustion study, this simpler ChemKin model was compared to three more advanced models who take into account respectively with nine, ten and fifty-three species, the first two including most, if not all, of the possible species in regard to hydrogen combustion and the third one comprising of all the species and subspecies needed for a methane/hydrogen mixture combustion (Kazakov & Frenklach), (Sa, et al., 2025).

The last model considers over three hundred reactions, so it definitively goes over the requirements of this study, but it was useful to run one single time to understand the number of species needed by the model and which ones had a greater impact on the combustion and the convergence of the simulations.

The first two models considered were either part of the Ansys Fluent ChemKin database, it being the H2_mech_NOx mechanism, or developed independently by other researchers, like the O'Conaire mechanism (Benim, 2024), (Daurer, Schwarz, Demuth, Gaber, & Hochenauer, 2024).

4.2.2 Eddy Dissipation Base Model

This model is the simplest considered in this study, given that it assumes that the reaction rate and the turbulent mixing rate are of different orders of magnitude, therefore the model follows the principle "mixed is burnt" (Vilag, Vilag, Carlanescu, Mangra, & Florean, 2019).

The chemical reaction rate is directly proportional to the inverted mixing time or respectively to the mixing frequency. This means that has soon as the hydrogen and oxygen reach the desired concentrations the reaction occurs instantaneously, and the chemical reaction properties are not considered.

4.2.3 Eddy Dissipation- Finite Rate

The ED-FR is an evolution of the Base Model, where the turbulent mixing is given by the ED BM while the chemical kinetic reaction rate is explicitly calculated from the Arrhenius formulation (Funke, et al., 2012). The mixing rate and the chemical rate are then compared to find the smallest one which is deemed as the limiting rate of the reaction (Daurer, Schwarz, Demuth, Gaber, & Hochenauer, 2024).

This model appears to be effective also for low Damköhler numbers, but there are still doubt on its applicability for detailed reaction mechanisms. This is considered as a good starting point for the study, both for its stability and for the relative simplicity of the related settings.

4.2.4 Eddy Dissipation Concept

The EDC model is based on the concept of turbulence energy cascade that defines how the larger eddies evolve into smaller and smaller eddies and, only when the eddies have the dimensions of the Kolmogorov scale, finally they are dispersed in heat (Funke, Beckmann, Stefan, & Keinz, 2023), (Benim, 2024), (He, Yu, Kuang, & Wang, 2021), (Daurer, Schwarz, Demuth, Gaber, & Hochenauer, 2024).

The concept is that this model excludes the correlation between the larger eddies and the production of heat, and this means that, in the EDC model, the fine structures (smaller eddies) are responsible for both the release of heat and the mixing that happens at a molecular level (Sternin, Ma, Liu, Haidn, & Tajmar, 2019).

For this reason, the refinement of the mesh and the use of a suitable turbulence model is of even greater importance because the EDC model actively depends on both to give back plausible results (Wartha, Bösenhofer, & Harasek, 2020), (Cheng, Zong, & Zhu, 2024).

Furthermore, the model is considered computationally costlier for the reasons expressed in previous paragraphs and this limits the use of the model to only when the better accuracy is adjuvated by a limited computational weight.

4.2.5 Flamelet Model

The flamelet models are based on the idea that every turbulent flame can be studied as an ensemble of small laminar flamelets, this model is computationally costly when compared to EDM, but still cheaper than EDC (Kumar, 2021), (Farabi, Ismail, & Abtahizadeh, 2021).

This means that the thermochemical state of the flame, and thus the one of the reactions, is described by the mixture fraction and the other variables in the same way it would be described in a laminar flame. Furthermore, the scalar dissipation rate is considered to account for the straining of the flame in the direction of the flow field (Porcarelli, Kruljević, & Langella, 2023).

The Flamelet model is regarded as stable and dependable, and it represents a good alternative to the ED-FR model (Zubanov, Stepanov, & Shabliy, 2016). A very similar model has been developed with the intent to track the progress variable of the

combustion in each flamelet, this model has been called Flamelet Generated Manifold (FGM) (Sa, et al., 2025), (Kumar, 2021).

The FGM model is different from the flamelet model because the variable of scalar dissipation rate is substituted by a progress variable. The two variables therefore depend on different processes to be calculated, creating differences in the predictions.

4.2.6 Probability Density Function model

This model is based on the assumption that the complete thermochemistry of the combustion can be described through the fuel mixture fraction (Posch, et al., 2025).

It is computationally costly to solve because it needs to solve special PDF-transport equations that are based on the conservation of mass equation. It is also necessary to have information about the neighbouring cells and that is why the Monte Carlo method is used.

There is another kind of PDF called Presumed-PDF which simplifies every distribution to a gaussian of beta type distribution, simplifying the calculation. It is usually used in combination with the flamelet model, and it is decidedly faster from the numerical perspective.

5 SIMULATION ON THE SINGLE BURNER

5.1 Test Rig Configuration

The data used for validation was obtained through experimental tests on the rig visible in Figure 10. In the first image it is visible the setup to supply the from both sides to create the air plenum, with isolating material surrounding the pipes to stabilize the temperature and limit the heat losses to the external environment.

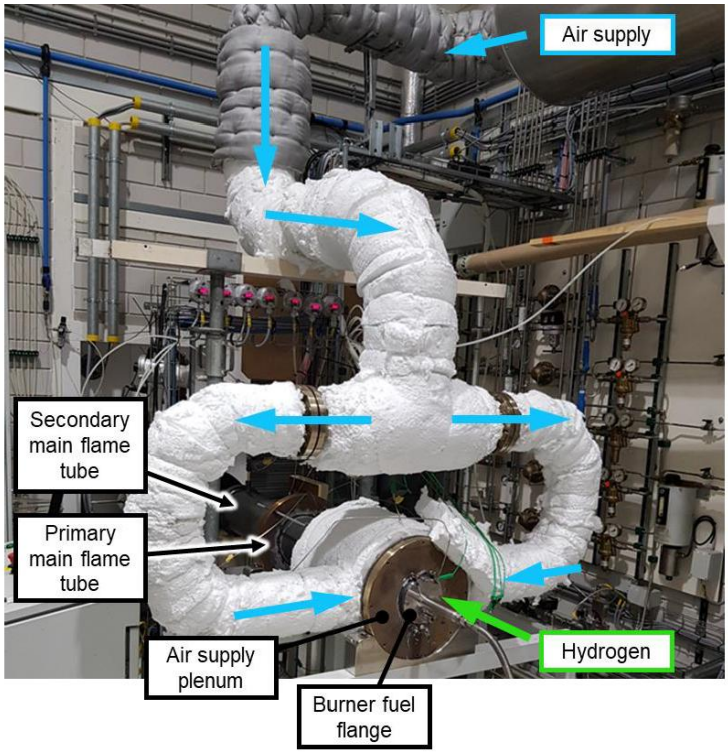

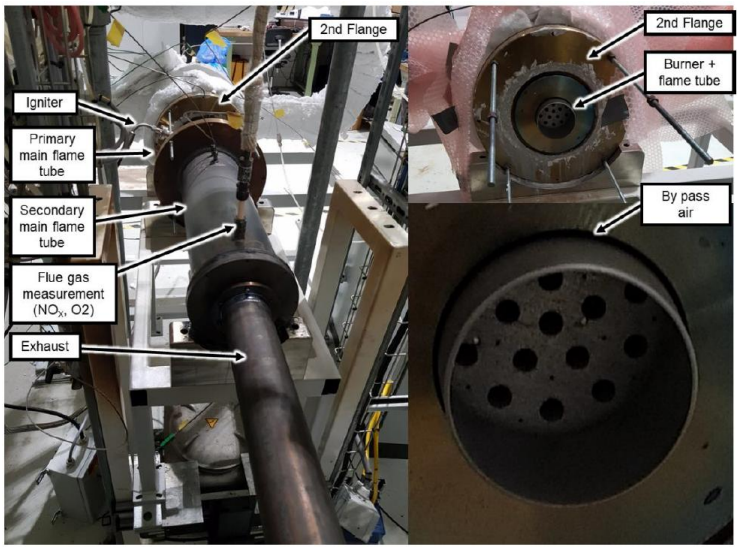

Figure 10 Test Rig

The burner was composed of sixteen units with five injectors each, and it is possible to notice the air bypass present outside of the circular case of the burner.

The second flange that contained the burner is connected to the primary main flame tube where the combustion started and propagated down to the secondary main flame tube.

The products of the combustion then flowed towards the exhaust where sensors were positioned to record the concentration of H_2, NO_x and O_2.

Other sensors were positioned at the intakes, in the combustion chamber and at the outlet to be able to record temperatures, pressure, mass-flows and power produced, so that the results could be used to validate the CFD simulations.

5.2 Reference case in Fluent

The model considered is a section of the burner, defined as Single Burner, which includes the pipe that functions as air inlet, intersected by five radially positioned inlets for the hydrogen. The air pipe has a circular shape, and the inlets are distributed on this profile. Compared to the model described above, this single burner does not have the Air Guiding Panel, meaning that the shear layer will be located between the incoming air flow and the recirculation vortex on the side of the wall. So, the turbulence and the vortices produced will be different and it will have to be considered when evaluating the performance of each model of turbulence and combustion.

The inlets and outlet were highlighted with, respectively, blue and red arrows. The part with the circular section is referred to as the burner, in which the JICF develops and the main part of the mixing occurs, while the second part is the combustor, where the flame propagates and creates NO_x emissions.

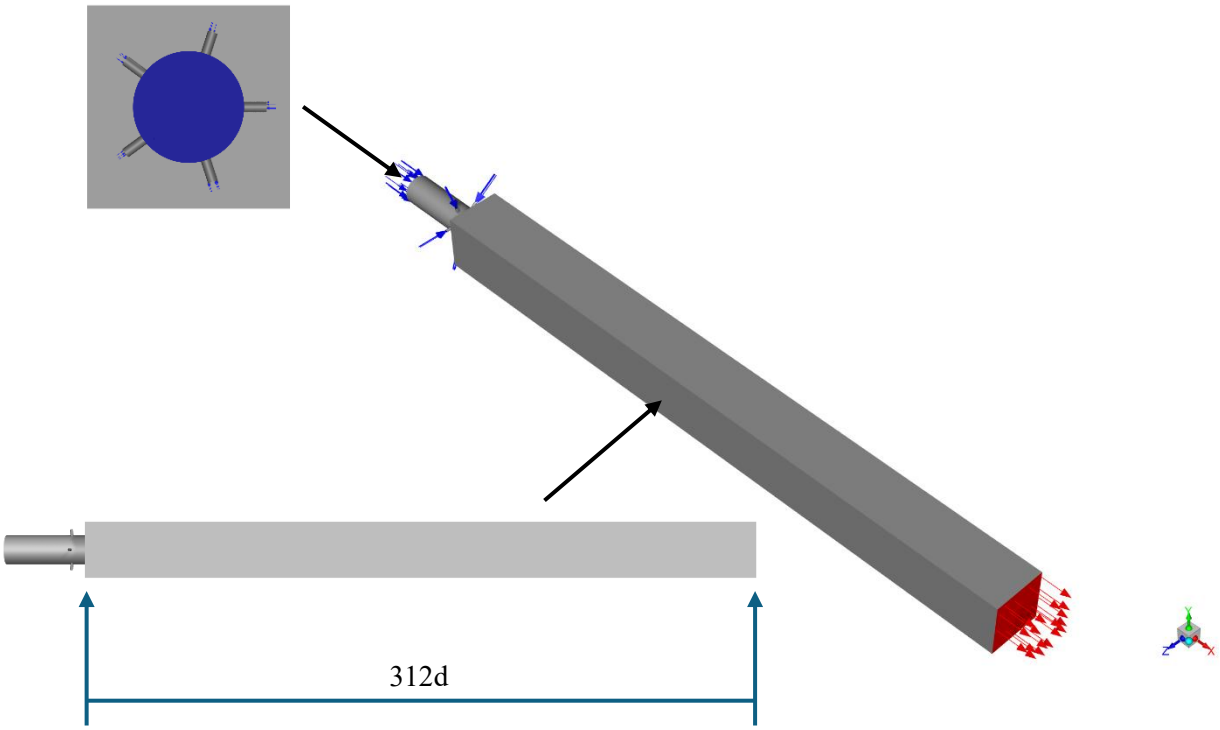

Figure 11 Model

The meshing was performed separating the design of the burner in different zones of interest, and the mesh gets coarser proceeding towards the outlet. So, the finer mesh was implemented in the air pipe, the fuel inlet and the first part of the burner where the flame would have theoretically developed and then the cell size would have got bigger where the gradients were lower or not important.

This choice was made so that we were able to optimize the speed of the calculations, without sacrificing the precision of the prediction of the behaviour of the turbulence in the combustion chamber.

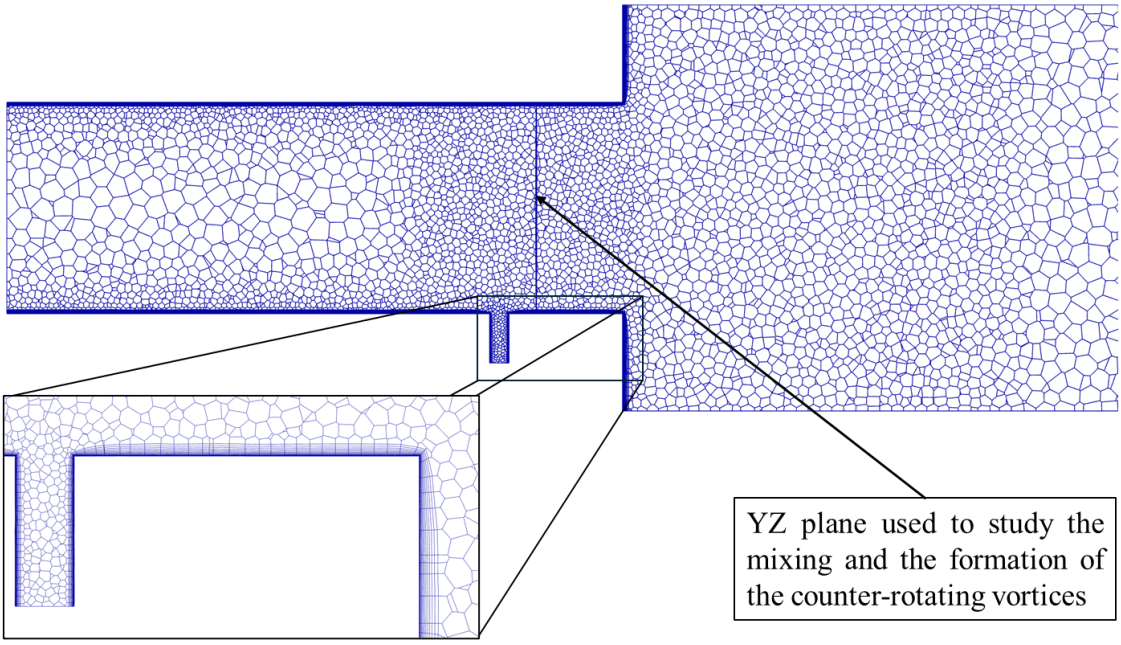

Figure 12 Initial Mesh (M1)

Different meshes have been compared to find the most suitable one for all the subsequent simulations (Charoenchang, 2021); for this particular application what would be important is the correct prediction of the turbulent flow at the fuel nozzle and the related mixing. From this prediction then the next step would be to check which model has the best behaviour during the combustion, therefore, the meshing needs to have the focal points on the areas of interaction of the two flows and on the area of combustion downstream. These requirements guided both the creation of the mesh and the refinement of it, indicating where and how the refinement of the mesh could have helped in the prediction of the burner's behaviour.

The different meshes retained the same initial settings, and, as reported in Table 3, were then refined in the above-mentioned areas. The reference models for turbulence and combustion were used to have a one-to-one comparison of the different meshes and their difference in behaviour. The results were then plotted, and a logarithmic behaviour of the results should have been observed from the coarser mesh up to the finest one, while the mesh chosen was ideally the intermediate mesh which gave results close to the finer meshes without being computationally heavy.

The initial conditions and the boundary conditions were derived from the experimental test and the inlet mass-in-flows were chosen to be the ones corresponding to the design

operating point of the burner. To make sure that every boundary condition was accounted for, the lambda of the mixture was computed and compared to the test value, which was measured with mass-flow sensor at the entrance of the inlets.

	Air mass flow ratio	Fuel mass flow ratio	Lambda	Air temperature ratio
REFERENCE	1,000	1,000	2,243	1,000
TEST3	1,010	0,870	2,604	0,998
TEST2	1,024	0,667	3,446	0,999
TEST1	1,039	0,478	4,871	1,000

Table 2 Operating conditions maintaining the airflow constant

The combustion model was defined modifying the coefficients of the Arrhenius rate of the single reaction:

$$2H_2 + O_2 \rightarrow 2H_2O$$

following the calculations realized in (Kildare, Evans, Tian, & Medwell, 2024). This was deemed necessary because the default settings of the Arrhenius formula were defined for a stoichiometric mixture and they created issues regarding the development of the flame, which started before the anchoring point, also representing a greater risk of flashback which was not observed in the test.

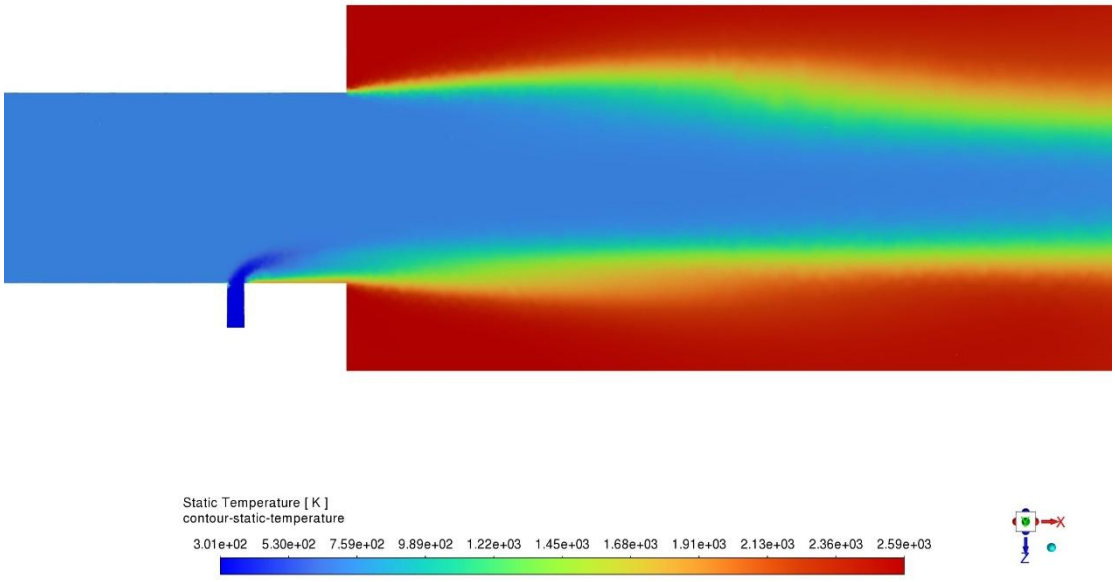

Figure 13 Ignition before the anchoring point

As it can be seen, right next to the fuel nozzle there was the development of high temperatures along the boundary layers which hindered the simulation and measurement of NO_x production downstream. Analysing the velocity magnitude in that zone we were able to notice that the flow was directed towards the outlet, it was, therefore, possible to exclude the possibility that this zone was subject to recirculation of hot gases from the flame region downstream. This meant that the higher temperature was due to the development of a proper flame in an unwanted zone and that the combustion model had to be modified to get rid of this effect.

The new Arrhenius Rate parameters were derived by interpolation of the ones presented in the studies (Li, Zhao, Kazanov, & Dryer, 2004), (Schiavone, Detomaso, Torresi, & Laera, 2024), (Mueller, Kim, Yettter, & Dryer, 1999) for the initial conditions of:

$$p = 1\ bar; T = Inlet\ Airflow\ T \text{ and } \lambda = 2.24$$

It is interesting to highlight how different Arrhenius rate models can be found in the literature, highlighting the difficulty in the definition of these parameters and their dependency on environmental conditions like pressure, temperature and the concentration of fuel and oxidizer.

It is also important to note that the following pages contain results obtained with a model which is private Intellectual Property, therefore some of the results will be reported through graphs and tables defined only by non-dimensional data and ratios, which do not disclose the specific data while being as effective in describing trends and overall behaviours of the models.

5.2.1 Mesh independence study

5.2.1.1 Local Refinement Method

Four meshes were created, each one containing double the number of cells of the previous one and the first having 300 000 cells (Long, Tian, Nathan, Chinnici, & Dally, 2015), which from now on we will define as M1 to M4 going from the coarsest to the finest mesh.

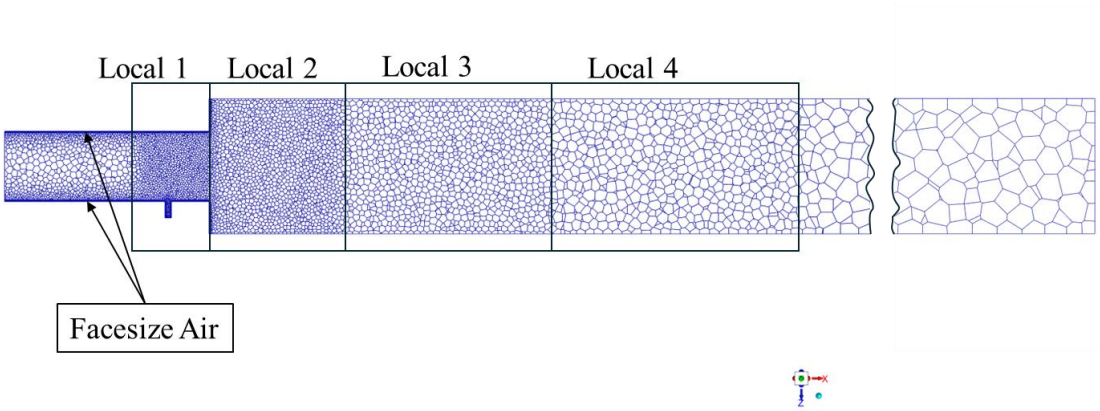

Figure 14 Local refinements regions

5.2.1.1.1 Mesh Settings

	Facesize Air [mm]	Local 1 [mm]	Local 2 [mm]	Local 3 [mm]	Local 4 [mm]
M1	0,2	0,3	0,5	0,8	1,2
M2	0,15	0,2	0,4	0,7	1
M3	0,15	0,15	0,3	0,6	1
M4	0,1	0,1	0,2	0,6	1

Table 3 Local Refinements specification

A set of different parameters were chosen to monitor the behaviour of the meshes and compare them to the others and to the test measurements: maximum temperature reached inside the combustor, average temperature of the gas passing through the outlet, the heat of the reaction produced and NO_x concentration in the exhaust gases. Given the slightly different layout of the experimental burner in Figure 10, which is composed of sixteen singular burners, the test data was used to validate the NO_x concentration results and the heat produced, while the temperature was less useful because of the final mixing of the products with the bypass air towards the outlet.

Furthermore, the NO_x concentration at the outlet had to be normalized to be comparable with the test rig that was equipped with a system of post-combustion air cooling which did not interfere directly with the production of NO_x, but it added air to the exhaust gases, skewing the measurement of the molar fraction of the NO_x produced compared to the RANS prediction. To generalize the results and compare them, the measurement of Oxygen at the outlet was used to define the normalized value of NO_x fraction in a mixture with a 15% fraction of O_2:

$$X_{NOx\_15\%O_2} = X_{NOx\ outlet} \cdot \left(\frac{X_{O2\ inlet} - 0.15}{X_{O2\ inlet} - X_{O2\ outlet}} \right) \tag{14}$$

The Ratios used for the representation of the results in the next paragraph are:

$$Max\ Temp\ Ratio = \frac{Maximum\ Temperature}{Inlet\ Air\ Temperature};$$

$$Out\ Temp\ Ratio = \frac{Average\ Outlet\ Temperature}{Inlet\ Air\ Temperature};$$

$$NOx\ Ratio = \frac{NOx\ prediction}{NOx\ measured};$$

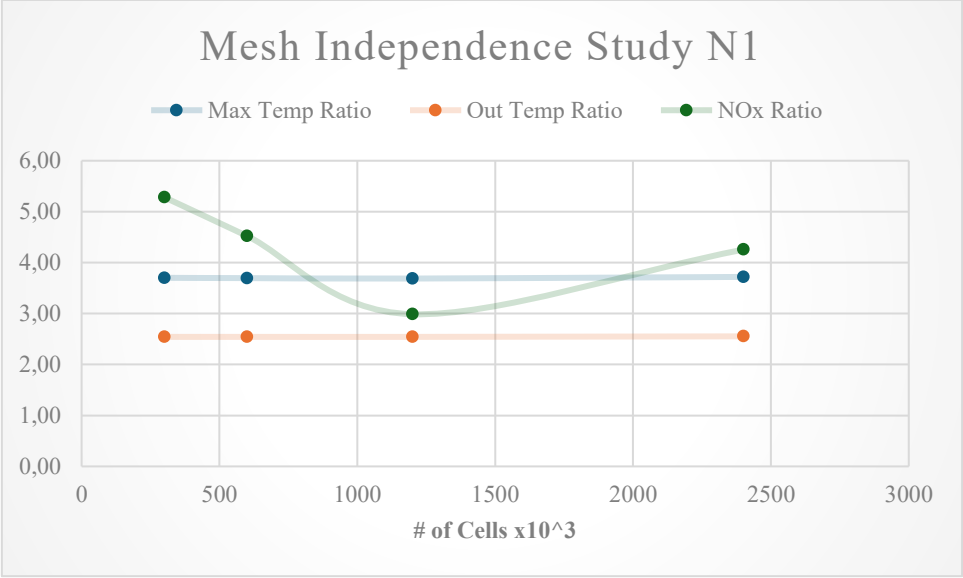

Figure 15 Post-processing results of the first meshes

It was also deemed important to evaluate the capabilities of the various meshes to predict the creation of the vortices at the fuel nozzle, so three contours were created on

different planes to visually study the mixing and the distribution of the Mass Fraction of Hydrogen.

The study was developed, and the first important observation was that the maximum temperatures in the volume and the average temperature at the outlet were stable for all the meshes, showing how the overall behaviour of the combustor was well predicted even for the coarsest mesh. The real difference laid in the NO_x production, where the mixing and the different air/fuel ratio at the beginning of combustion yielded different results.

The trend from the meshes was not the one predicted by the theory, with a higher NO_x production for the finer meshes and overall, no convergence could be appreciated by the first four meshes.

This behaviour was not ideal, and the principle behind it was that, with a finer mesh, especially in the flame region, the possibility of having peaks of temperature, which would then cause a higher NO_x production, was lower. Thanks to the visual study of the vorticities, it was possible to make different observations related to the mixing.

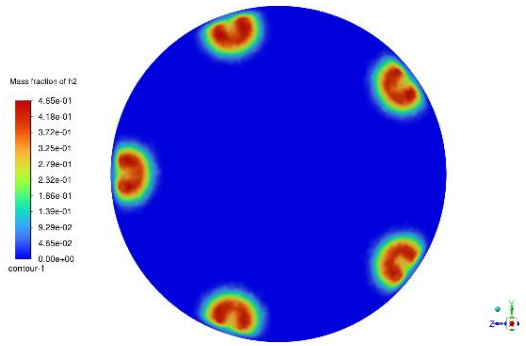

Figure 16 Mass fraction of H_2 for M2

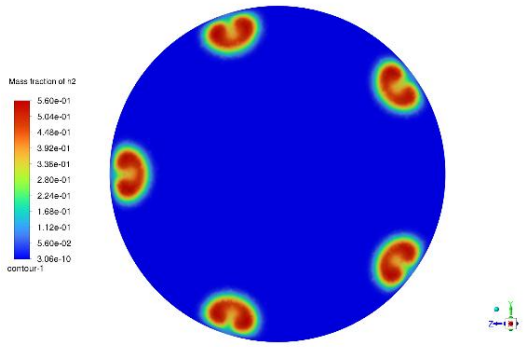

Figure 17 Mass fraction of H_2 for M5

Numerous sources from the literature agreed that the main difference between the turbulence at the nozzles predicted by RANS models and the referenced behaviour was that the RANS models predict that the mixing and the vortices stabilize while, in reality, the mixing at the nozzle is chaotic and that also usually results in higher mixing rates which are not easily predicted by RANS models.

The prediction of the turbulent mixing in the reference case with various meshes was deemed as accurate, as it was possible to recognize in all three planes the characteristics of the Jet-In-Crossflow described in the Theory part of this manuscript. The Figure 16 and

Figure 17 displayed the development of the counter-rotating vortices on the YZ plane referenced in Figure 12.

It is important to note from Figure 15 that the k-ω SST model would have needed in any case some kind of tuning, as the normalized values of NO_x were not comparable

with the ones measured in the test rig. This tuning was, however, postponed and a study of the model was developed to understand what could have caused the worsening of the prediction with the finest meshes.

It was evident from the Figure 16 and Figure 17 that the coarser mesh predicted a faster mixing, as the concentration of H_2 was lower in the vortices compared to the other mesh, meaning that a greater amount had already mixed with the air. So, even though the mesh should have been less accurate, the mixing that was generated described more accurately the referenced behaviour of the JICF. This result would have been in line with the assumption that the RANS models overestimate the turbulent viscosity and, in so doing, underestimate the turbulent mixing. This created a situation where the refinement of the mesh should have asymptotically converged to a wrong value, while the least precise value approximated the best the real behaviour.

To solve these issues the first attempt made was to add two more meshes with a higher refinement to observe if the meshes' results would eventually converge, but even these simulations gave a disappointing result as it could be observed an improvement in the prediction of the NO_x production, but there was no convergence for these improved predictions.

The study of the vortices needed to be combined with the ones regarding NO_x, where M5 and M6, albeit having significantly slower mixing than M2, outperformed M1,2,3 and 4 to have the lowest production of NO_x.
Theoretically, the faster mixing would have assured an even distribution of the fuel in the mixture, avoiding hot spots and area where the mixture is near stoichiometric, but in this case it is plausible to assume that the lower number of cells present in the flame area meant that artificial peaks of temperature were measured and, consequently, the NO_x production resulted higher with the use of M1,2,3 and 4.

The NO_x production was, in any case, not even remotely comparable with the test values measured, as it was overpredicted by an order of magnitude. When trying to design the best mesh layout, so that the model could come close to those values, it is easy to understand how the characteristics of M1 and M2 in the mixing zone would have been complementary with the flame region properties of M4 and M5 in creating a mesh which had the closest results to the real ones.

This idea might be applicable to a singular geometry with only a handful of operating points, but it is not ideal when a multitude of operating points is considered and especially when the study is aimed at singling out characteristics of the turbulence and combustion models.

So, delving deeper into the study of the mesh was important to eliminate the mesh dependency from our models and to completely eliminate every other source of

inaccuracy. It was, therefore, crucial to understand which mesh was precise enough to approximate the asymptotic behaviour of the finest meshes while also being of a manageable size itself.

As mentioned before, the ideal predictions of the mesh should have converged towards an asymptote for really fine meshes and the choice of the mesh to be used for all the simulations should have been driven by the closeness to the asymptote in proportion to the mesh size. In this case the simulations with the first four meshes were inconclusive, so the comparison of the additional meshes gave other points of discussion.

5.2.1.1.2 Comparison of M2, M4 and M5

Three meshes were first compared and post-processed to understand their different characteristics: M2, M4 and M5 were analysed considering various contours which gave away a lot of information. The comparison of the Static Temperature contours was probably one of the least useful, because of the extremely similar behaviour of flame and the same temperature development inside of the combustor. The only appreciable difference was the higher penetration of the cold jet of Hydrogen in the finer mesh M5.

When considering the NO rate, the result of the mixing is that the NO production is more evenly distributed in M2 compared to M4 and M5 which have highest peaks of production. Every mesh also presents NO production in the hot recirculation zone, but the problem is much bigger for M2 and M4 than M5. This cements the observation that M4 finds itself plagued with the inaccuracies, higher NO rate peaks and hot zones not under control, of both M5 and M2 without having any of their advantages.

As previously stated, the coarser mesh ensured the faster mixing, but from the study of the mass and molar fraction of H_2 it was possible to make other observations:

1. The coarser mesh had limited accuracy in the prediction of the behaviour of the horseshoe and leading-edge vortices.
2. The finer mesh M5, interestingly, predicted less air bleed into the fuel pipe on the leading-edge side compared to the coarser meshes.
3. The slower mixing in M5 also made the H_2 diffusion zone longer and thinner, while in M2 the zone is larger in the vertical direction and risks to interact with the other injectors' zones provoking the undesirable phenomenon of flame merging.

The interpretation of the differences between the meshes for the Heat Release was unclear: in M2 the Heat Release was more evenly distributed, having appreciable levels of heat being released from the anchoring point until the Primary Heat Release Zone,

which is located towards the middle of the burner, while in M4 and M5 the Primary Heat Release Zone was much more prominent. Furthermore, it was noticeable that the Heat Release of M5 was much better distributed and with a less steep gradient than M4, while the peak of Heat Release was higher for M4 than M2.

The Rate of Reaction contour underlined how the difference of refinement was even more visible when taking into account the thin layer of cells where the primary reaction zone was. Regardless, it was also noticeable how, even in M5, the Rate of Reaction presented peaks, and the distribution was not as linear as it should have been. This meant that the next step of mesh refinement would have had to take into account the small slithers of cells in which the reaction occurred to make sure that the Rate of Reaction was best predicted.

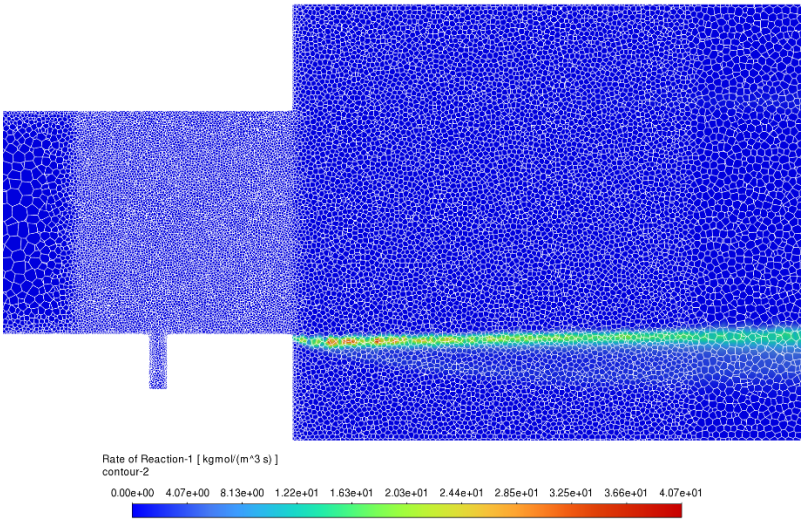

Figure 18 Rate of Reaction of Mesh 5

Two methods were discussed to enhance the prediction capability of the mesh in those models: the first consisted in the modification of the model to include an internal cylinder as the continuation of the air pipe, which would have been considered as an "internal" boundary, meaning that it wouldn't have affected the flow, while also being the starting point for a Facesize refinement. The second option was relying on Fluent function of "Manual Adaption" thanks to which it is possible to choose a parameter or variable to determine if a particular cell would be refined.

5.2.1.2 Manual Adaption Method

Because of the simpler approach, the second method was tested first, setting as the parameter the Rate of Reaction itself and limiting the gradient between adjacent cells, the result was that a refinement was developed for the wake of the five injectors after the anchoring point, effectively limiting the excess in refinement in other zones of the mesh.

When the manual adaption was first set up, it became also evident how the second method would have needed some modifications to become feasible to implement because the reaction did not develop parallel to the walls of the burner, but it slowly developed towards the centre, rendering the cylinder approximation majorly inaccurate.

The first attempt was made adapting and refining all the cells that presented a high gradient in the Rate of Reaction, trying to avoid the peaks present even in M5. The adaption was developed for the cells which presented a gradient in the Rate of Reaction in 99th percentile which were confined in a limited area downstream of the anchoring point.

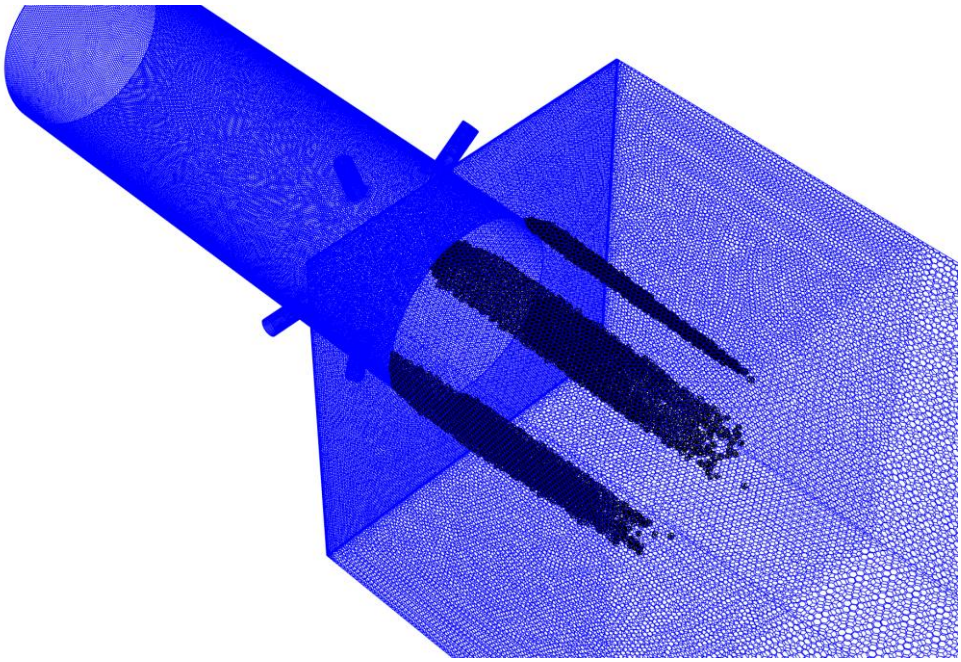

Figure 19 Adaption cells for Rate of Reaction

Unfortunately, the first result with this adaption were not successful as we would have hoped, and it was highlighted once again the high mesh sensitivity presented by the model.

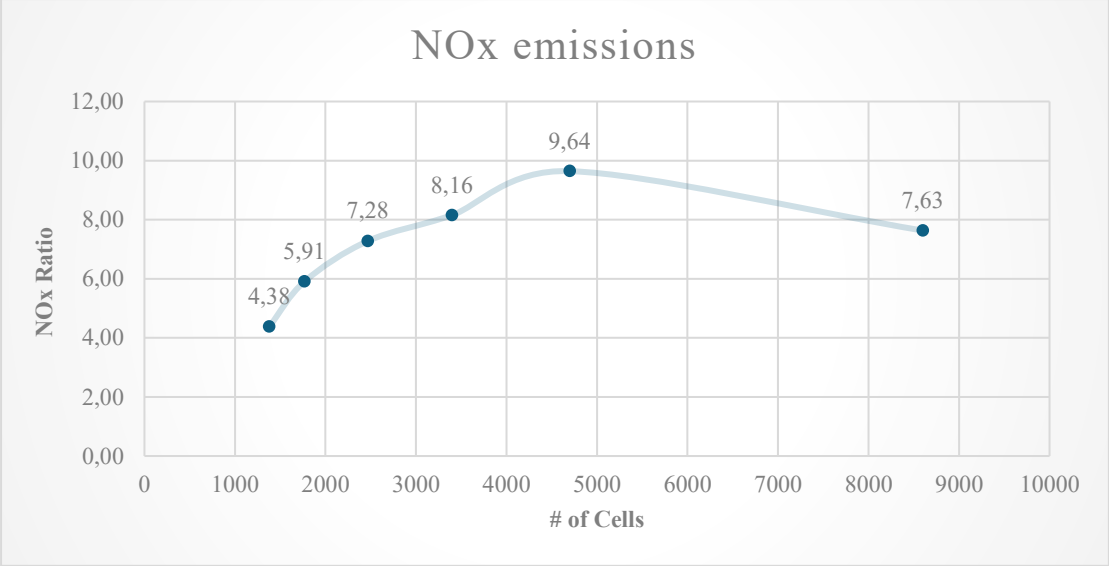

Figure 20 NO_x Emissions for each Mesh

The interpretation of the results was not as straightforward as we would have hoped and, while the temperature measurements were quite stable across all the six meshes, it was not the same for NO_x production that first worsened with refined meshes and then started to decrease again for the finest ones. This was not an ideal behaviour that also combines with the fact that the results, even for the finest mesh, are far from predicting a NO_x production close to reality.

Even though the first attempt was not successful, it was evident how this method of "Manual Adaption" represented a convenient tool to make sure that the refinement would be confined to zones of high interest, the task was now to highlight all of these zones and account for them in the meshing.

Even multiple rounds of refinement of that area could not avoid the development of peaks of reaction, that seemed to develop regardless of the refinement in that area, so it was deemed necessary to add another round of refinement upstream of the Reaction Zone, to take into account the mixing from the inlet to the former.

The proposed correction took into account the prediction of the vortices of the JICF, adapting and refining the areas in which the ratio between the concentration of O_2 and the concentration of H_2 was inside the range of flammability. This adaption would have considered the mixing and the Rate of Reaction at once, but unfortunately the area in which the combustion was possible was much larger than the one in which the flame would actually develop, rendering this refinement ineffective especially for finer meshes, as it represented an exponential increase in mesh size.

A smaller range of H_2 concentration was considered, only adapting the first part of mixing that had higher H_2 concentration from the fuel injectors to a point fixed 20 mm after the expansion of the burner. In this way the hope was to accurately predict the mixing without weighting the model down with an over-adaption in undesired zones.

After the simulation, another adaption was performed to take into account the Rate of Reaction and a third one was then developed to distribute peaks of NO production in the flame region. These three consecutive adaptions were deemed a suitable combination that considered the mixing, the onset of the reaction and the NO production with the slimmest model possible.

The first simulations started from the adaption of the known meshes and the results were still disappointingly unconclusive, with no clear convergence and growing NO_x production for finer meshes. To understand better the effect of each adaption, simulations with and without the NO rate adaption were analysed.

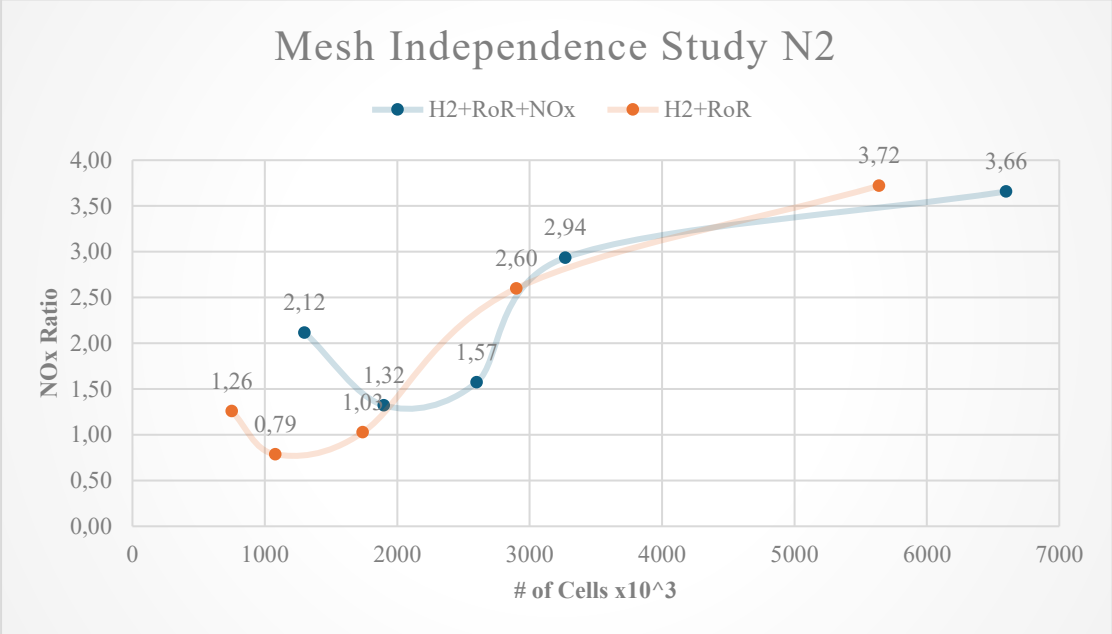

Figure 21 Emissions with two types of Mesh Adaption

From this study, it was evident that the behaviour of the five meshes was almost constant and that the adaption regarding the NO rate has the consequence of stabilizing the results for finer meshes getting close to the wanted convergence. Still the behaviour of the first meshes was not ideal and the strategy set was to simplify the initial meshes to check for inaccuracies in the definition of the cases, while also making the models slimmer to eventually implement a second adaption of the NO production rate.

The local refinement regions were scrapped to implement only one zone which included both the mixing and the combustion zone, this was done to eliminate possible inaccuracies of the previous meshes which had a variation in cells density between those two zones. Other six meshes were created and the refinement of the region was upped each time to obtain an exponential growth in the number of cells, as it is advised for Mesh Independence studies.

The simulations for each one of the meshes were organized in different rounds of run and refinement, in the first round after having obtained a convergent behaviour of the results, the model was refined in the mixing zone, then consequently the same was done for the Reaction zone and the NO_x production zone.

It is important to remember that the different refinement level of the meshes gave very different results for the mixing before the adaption cycles, so, also the range of H_2 taken into account would have to vary among the meshes because of the different initial mixing predicted, to maintain the same area of adaption. The other rounds of optimization, for the Rate of Reaction and NO production rate, showcased a higher level of stability and smaller variance compared to the H_2 range.

It was predictable that the coarsest mesh could not be accurate, starting the adaption from a really coarse mesh, but it surprisingly gave results remarkably close to the finer meshes, probably evening out its defects in the reaction zone with its benefits in the mixing zone. The results, compared to the previous simulations, are much closer and the finer meshes appear to have converged towards a value of NO_x of 1.5 times higher than the real value measured during the test. For the finest mesh it was considered the average of the last twenty operations, given how it was exhibiting a slightly oscillatory behaviour in the NO_x production results.

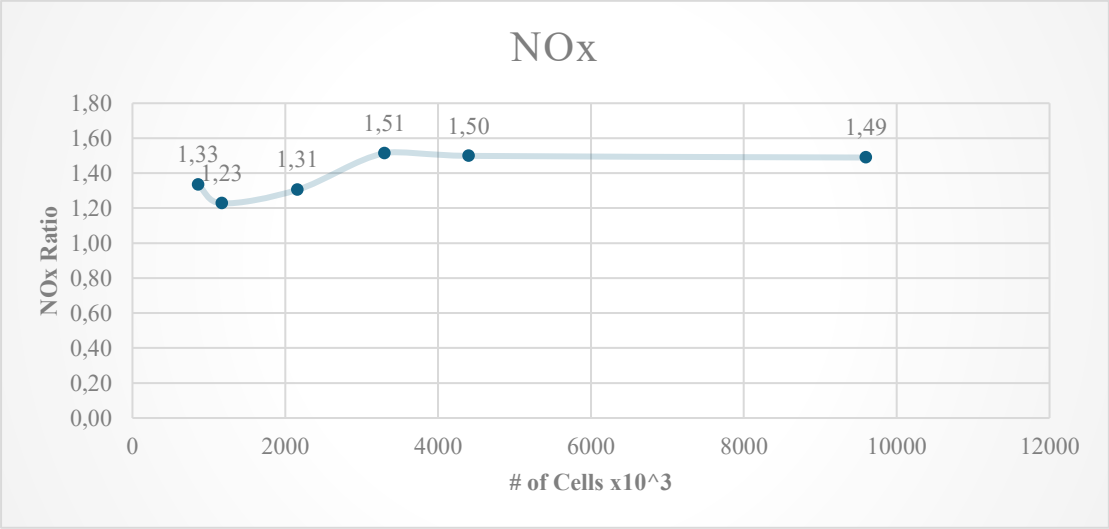

Figure 22 Mesh Independence study completed

The finest three meshes converged towards this value, which is also close to the test result compared to the previous attempts, considering that the only tuning done up to this point was the modification of the Arrhenius Rate to obtain the right behaviour of the flame. Therefore, it was possible to utilize M5 for the next simulations (4.4 million cells), given how it is represented the results well while also being the less computationally costly.

Developing this study further, it was always clear that this method of mesh optimization presented the limit of having to adapt the meshing through simulation, so it could not be implemented all at once, but every model would need to be tuned various times so that the consecutive adaptions would be the most appropriate.

This adaption could be used also for other geometries to retain the mesh independence, so it was necessary to understand the level of refinement which would be optimal for each case. For this reason, a parameter was developed as the ratio between the cell size in proximity of the fuel injector and the diameter of the fuel injector itself.

The Area-Weighted Average of the Cells size in the region was used to derive the characteristic length of the mesh, in this case defined as the radius of the average cell, assuming it to be a sphere. This characteristic length is then divided by the injector diameter to define the ratio R2.

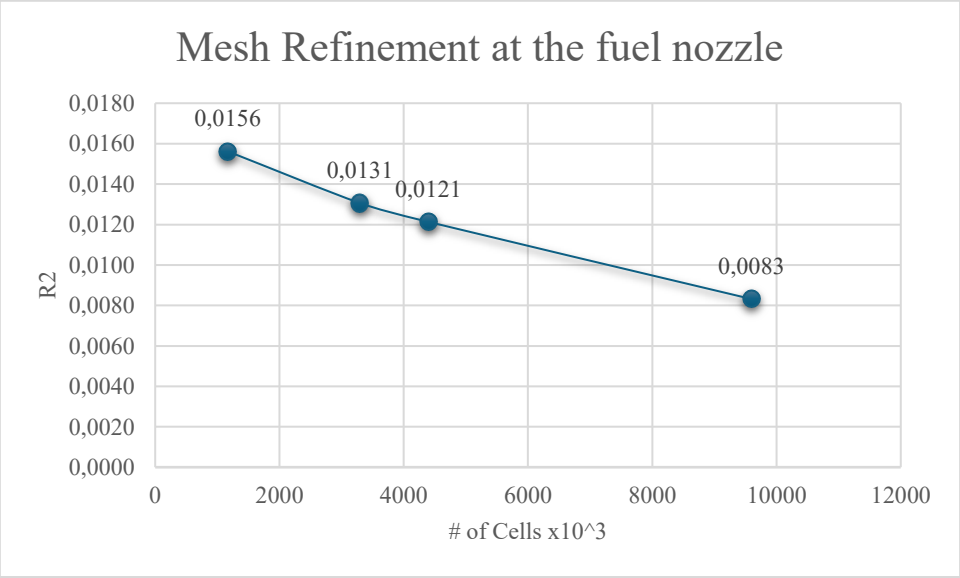

Figure 23 Trend of the ratio R2 plotted against the Cell Size of each Mesh

The idea behind this analysis was the possibility that these results could highlight the minimum ratio that gave a refinement of the mesh sufficient to accurately describe the model. Another study could have been developed to ensure that this measurement could have been directly transported to other geometries, but that was not the focus of this report.

Another important step would be to check how this mesh behaves for different initial conditions; there is the need to understand if the mesh is optimized for each one of them or if subsequent tuning is needed. It is important to note how two different routes could be taken in this regard: the first would be the simulation with the mesh obtained for the reference case, while the second would be the adaption of all the initial conditions with different meshes using the original design method.

The two possibilities have different aims because for the first, the simulations would be useful to understand how the single mesh behaves for different situations, while for the second, the adaption of the mesh would be useful to the check the mesh independence study in another initial condition, and to finally pronounce if the method chosen is reliable with different models.

Using the same exact mesh, the results were not the expected ones, and the reduction of the fuel flow did not yield lower emissions, as we can observe in Figure 24Figure 22 the behaviour of the mesh was not ideal, and no real trend could be extracted from it.

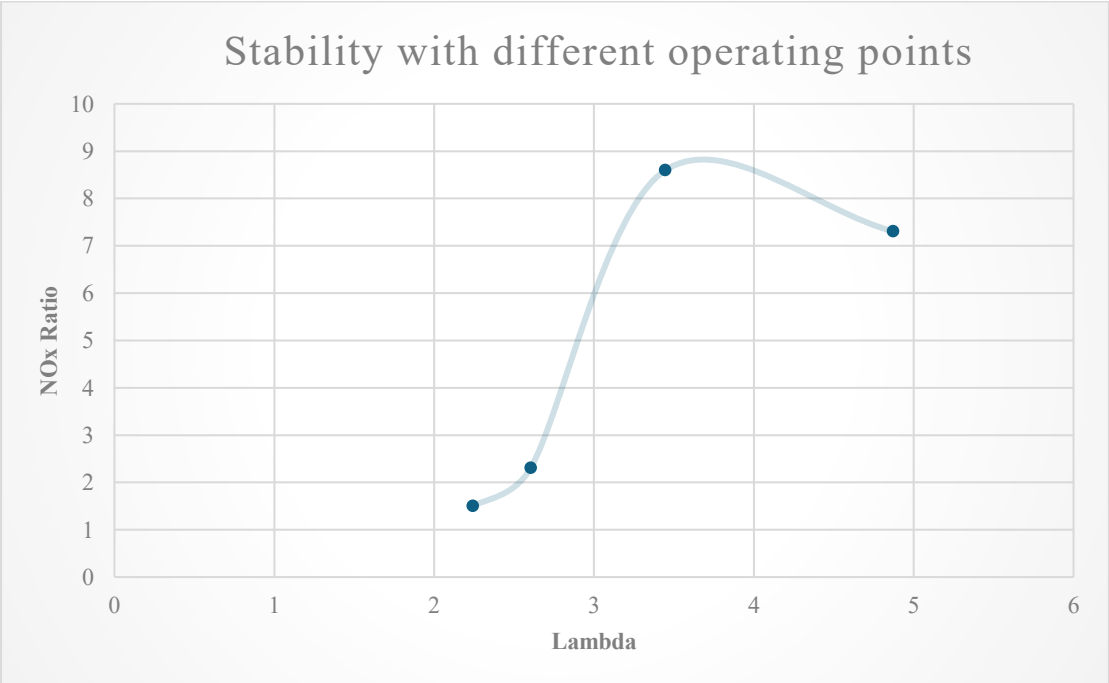

Figure 24 NO_x emissions for the same model and different lambdas

An argument was made for the limitations of this approach related to the instability of the adaption and the continuous need for a subsequent adaption in critical regions. Another criticality of this method would have been the high uncertainty that the mesh would inherit after a series of adaptions that have a small, but not negligible percentage of error.

The meshes obtained in different runs would therefore vary and there was no way to analyse the possible effect that these variations would have had on the results of the simulations. For these reasons, this approach was abandoned, and a new one was considered.

5.2.1.3 Refinement Volume Method

Another model was taken into consideration, in which the CAD model was modified to include a new volume that would be the base for the refinement. The volume can be described as a thickened pipe long enough to include all the area of mixing and reaction inside the burner. This solution was implemented to eliminate the possibly critical difference in mesh density that was initially setup between those two areas.

The idea was to utilize this volume to describe other two refinement regions: Bodysize inside the volume, which refines the volume to the required mesh size, and Facesize on its faces which refines the surfaces and assures a smooth transition between the small cells inside the volume to the bigger ones outside of it.

The volume is then defined as a "dead region" which is not considered in the final Volume Meshing, therefore impeding every disturbance in the final mesh and subsequent models.

The mesh created was modified into four variants in which the difference lied only in the level of refinement of the newly created volume, using the previous simulations as a starting point to decide on the refinement needed for the four meshes. As it can be seen in the Figure 25, the model would need a larger number of cells than the "Manual Adaption", but it would also be less likely to display instabilities throughout the simulation.

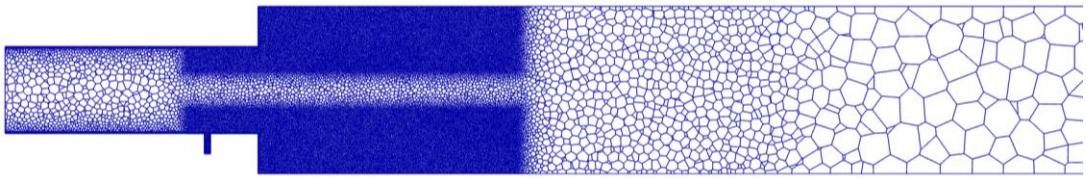

Figure 25 Refinement Volume applied to the Mesh

Unfortunately, it was evident from the first run that the Arrhenius Rate, which had been developed for the previous model, was not ideal for this application, as it was probable that the mesh problems had also repercussions on the decision of the parameters for the Rate of Reaction's formula.

The problem was related to the over prediction of the Rate of Reaction that caused the combustion to develop before the anchoring point and for the development of hot backflow up to the fuel injectors (As in Figure 13). For this reason, the Arrhenius Rate

was modified to obtain again the expected behaviour, without a total dedication to the tuning and optimization of the pollutant emissions.

A suitable Reaction Rate was derived from (Schiavone, Detomaso, Torresi, & Laera, 2024) and all the meshes were then tested with this model. Unfortunately, the model as indicated gave stable results only for the two coarser meshes, while maintaining a non-ideal behaviour for the finer ones. For this reason, it was necessary to slightly tune the model to obtain feasible and stable results with all the meshes.

Once modified, the model gave optimal results of convergence without any need for meshing refinements. It was noted that the NO_x emission converged to the wrong value, but the focus in this part of the study was just assuring that the emission results would be independent from the mesh. The mesh chosen for subsequent studies was the second finest one, which gave good results while being also relatively "light".

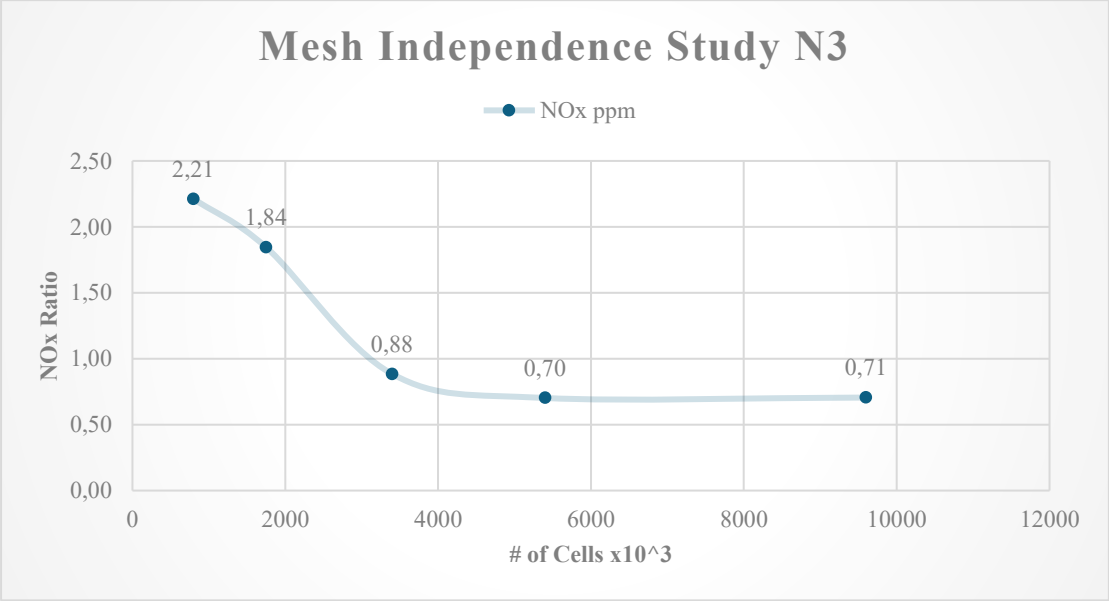

Figure 26 Mesh Independence Study with Refinement Volume

As it was done previously, it was then deemed necessary to focus on different operating points to understand if the model was able to describe the expected trends in NO_x production and temperature and to make sure that the mesh with the "Volume Refinement" displayed a better trend that the previous approach. The model was kept exactly the same without any modifications for these simulations, changing only the fuel flow for each simulation and the results can be seen in Figure 27.

One of the objectives of this study is to evaluate if the models implemented are capable of giving stable and accurate predictions for all possible conditions, so that it would be

possible to implement the same models also on other geometries and models, counting on an accurate prediction for both the turbulence and the combustion.

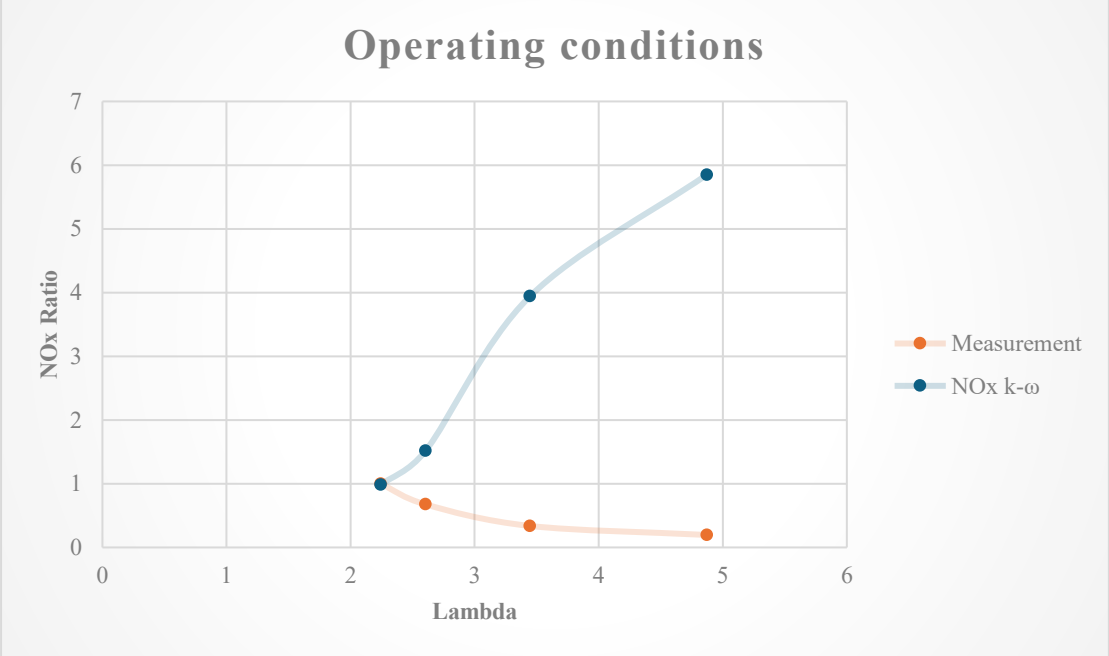

Figure 27 Comparison between the results of the Refinement Volume model and the Predicted values

It is evident that, once again, the results do not coincide with the experimental results, and the trend is the opposite of the expected one, with higher NO_x production for lower fuel flows.

Given that both the methods of "Manual Adaption" and "Refinement Volume" gave similar results distant from the ideal ones, it was deemed necessary to develop a post-processing analysis to explain this trends. The only difference between the two models was the result for the lowest fuel flow, with the former predicting a slightly lower value compared to the trend.

The linear behaviour of the second approach was considered more suitable to be analysed to find eventual evidence on the cause of such a different reading.
The first examined parameter was the Mole Fraction of H_2 inside the burner, with particular attention given to the initial zone of mixing for the reference case (*lambda*=2.24) and the case with second lowest fuel flow (*lambda*=3.45):

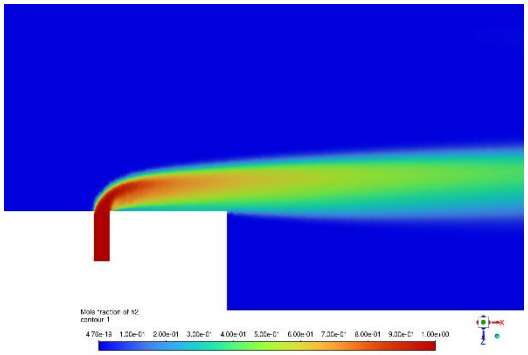

Figure 28 Mole fraction of H_2 of the reference case

The difference between the two meshes is evident when it comes to the penetration of the jet and the overall mixture distribution downstream of the nozzle.

The reference case has a higher mass flow and that is why the jet is able to develop further from the wall.

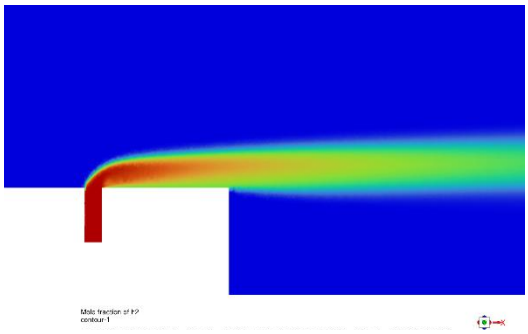

Figure 29 Mole fraction of H_2 of the model with reduced fuel flow

Even though the quantity of hydrogen was reduced in the second simulation, the mixing was seemingly not affected. Moreover, it was possible to observe how the flow of hydrogen remained close to the wall, as the parameter which influences the detachment from the wall is the crossflow injection velocity.

This behaviour would also have as a consequence the fact that the concentration of hydrogen at the anchoring point would be higher when the flow it still attached to the wall, resulting in higher lambdas in the reaction zones, higher temperatures and higher NO_x production as a consequence.

This reasoning was supported by the temperature measurements of the various simulations, in which it is possible to notice how, even though the temperature at the outlet diminishes because of the lesser amount of fuel, the maximum temperature grows and with that the production of NO_x. It is important to remember that the NO_x production has a quadratic dependency on the temperature, therefore the less fuel burned was outweighed by the much higher combustion temperature.

Given these results and the research in the literature (He, Guo, & Hsu, 1999), (Catalano, Chang, & Mathis, 1989), it was possible to verify that, especially for lower injection mass flows and for crossflows that attach to the air pipe walls, the mixing is highly dependent on the Turbulent Schmidt number and it is therefore not possible to assume that the model is able to reproduce different operating conditions maintaining the Schmidt Number constant.

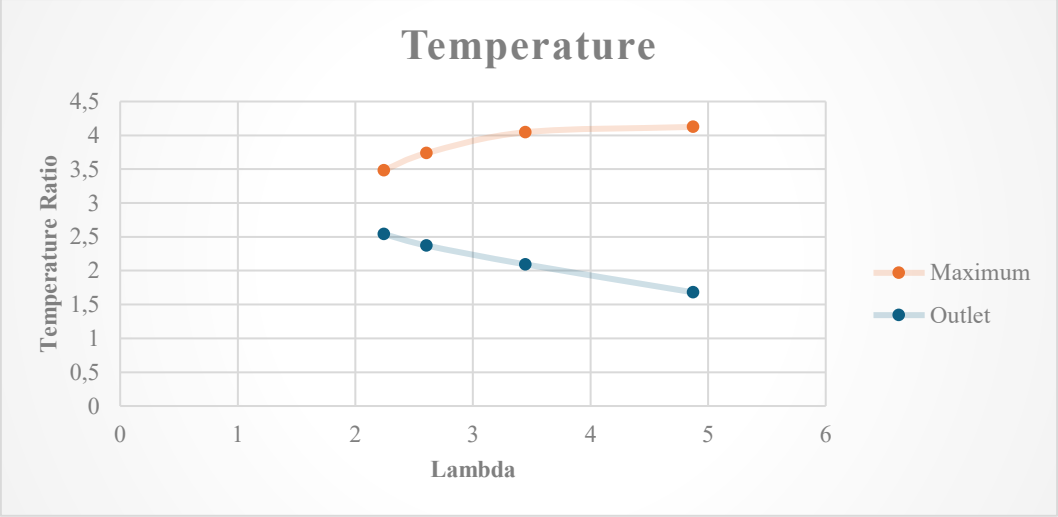

Figure 30 Trends of Maximum and Outlet Temperature for different fuel flows

The reference model was therefore considered not fit for our investigation, as it was evident how critical the mixing in the injection zone was, and it was not well predicted by the model for lower fuel flows. This means that, without proper tuning for each operating condition, the k-ω SST model cannot accurately predict all of the operating conditions. For the same reason, it was considered that also the URANS model would struggle with this problem and the first efforts were made on other turbulence models to understand if they are more capable or if the tuning of the Schmidt number must be considered as part of the set-up process.

5.3 Model Setup

5.3.1 Turbulence Model Variation

5.3.1.1 k-ω SST

Being this the reference model, it was used for the setup of the meshes. In the conditions for which the chemistry model had been set up, the turbulent model gave stable results that would assure the reach of the mesh independence, while predicting results fairly close to the experimental ones. This situation could not be replicated when focusing on keeping the inlet air flow fixed and variating the quantity of fuel flow, therefore, after the first simulations it was obvious that more operations of optimization were needed so that the model could be accurate for different air/fuel ratios.

The first option would have been to change the Arrhenius rate to accommodate for the variation of the initial condition but, observing the development of the vortices, it was also clear that there was another problem with lower fuel flows, which had a really small penetration into the burner, effectively preventing the model from predicting correctly the development of the known JICF vortices. This problem led to the research of a solution through the study of the turbulence model, without giving additional weight to the Arrhenius rate parameters.

This choice was also made to simplify the different models and try to standardize the use of a singular Arrhenius formula for all the turbulence and combustion models, also considering that eventual changes to it would have been the results of the study of three parameters simultaneously, which would have been a long and not error-free process. This choice was also supported by the understanding that the Arrhenius Rate of a particular reaction depends on different parameters that are related to the geometry, but not on the turbulence model of the model.

As previously mentioned, the attention has been focused on a single parameter present in the settings of the k-ω SST model, the Turbulent Schmidt Number, and the reasoning behind it is in the definition of the parameter, which represents the ratio between eddy viscosity and eddy diffusivity, the two being respectively the rates of turbulent transport of momentum and the turbulent transport of mass. The variation of lambda meant a reduction of mass diffusion with constant eddy diffusivity.

The study of the ideal Turbulent Schmidt Number for the models was the combination of try-and-error method with the help of reverse engineering for validation: when considering a specific set of inputs, the fuel flow was set as in the test data while changing the Turbulent Schmidt Number to match the turbulent behaviour and therefore the NO_x production of the test rig.

This method was used for one set of simulations, keeping the air flow constant and diminishing the fuel flow until 4 different operating points were individuated, and a pattern was outlined.

To evaluate if there could have been a trend among the chosen Schmidt Numbers, another physical quantity was defined as the Impulse Ratio:

$$IR = \frac{J_i}{J_{ref}} \text{ where } J_i = \Delta P_i \cdot v_i$$

(15), (16)

with J_i being the impulse at the fuel inlet for a particular condition, and ΔP_i and v_i being the dynamic pressure and the velocity magnitude always recorded at the fuel inlet.

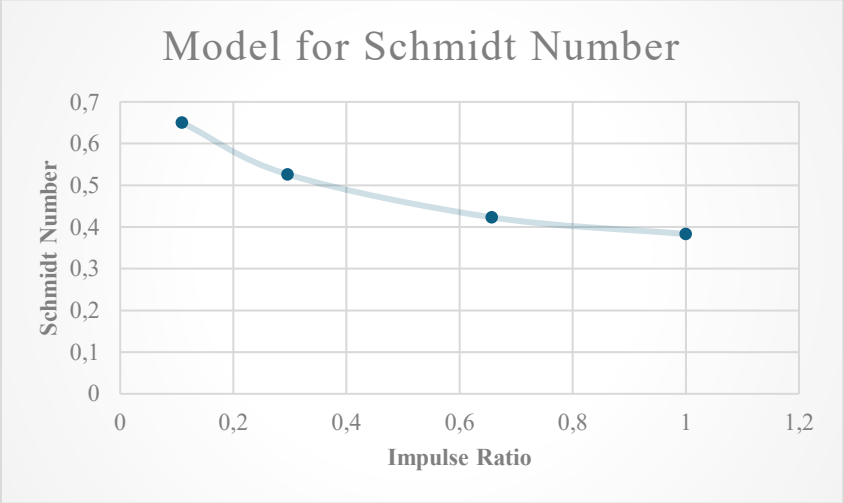

Figure 31 Schmidt Number setting needed to correctly predict the NO_x emissions for different impulse ratios

The behaviour of model seemed to be stable, and a clear trend could be outlined. This result would theoretically mean that, given a certain fuel flow for this model, following the curve depicted above, it was possible to tune the model to give out the test emissions for the particular airflow. This means that the model is capable of some flexibility without losing accuracy of the prediction on the functioning of the combustor, but the ideal behaviour would include the correct prediction with variation of both fuel and airflow.

Another important side of the study is trying to figure out generalized rules to apply even to different geometries that can render precise predictions before the introduction of testing.

Therefore, the next step would have been the validation of this results through simulations of different initial conditions retaining the same Arrhenius Rate and adapting the Schmidt Number to follow the curve found with the reference case.

Apart from the reference airflow, two other models with different airflow settings were studied to try to find a relation between the choice of Schmidt Number that gives the best prediction for NO_x, and the Airflow.

Unfortunately, the Schmidt Number used to tune the model in the design conditions was not the same for all conditions with the same lambda, therefore it was necessary to determine the right value of said parameter for each fuel flow to analyse the trend and try to predict the behaviour for other conditions as well.

Three different airflows were studied, each one having four different operating conditions. The trends observed were similar with only the exception of the lowest fuel flow for the lowest airflow taken into consideration.

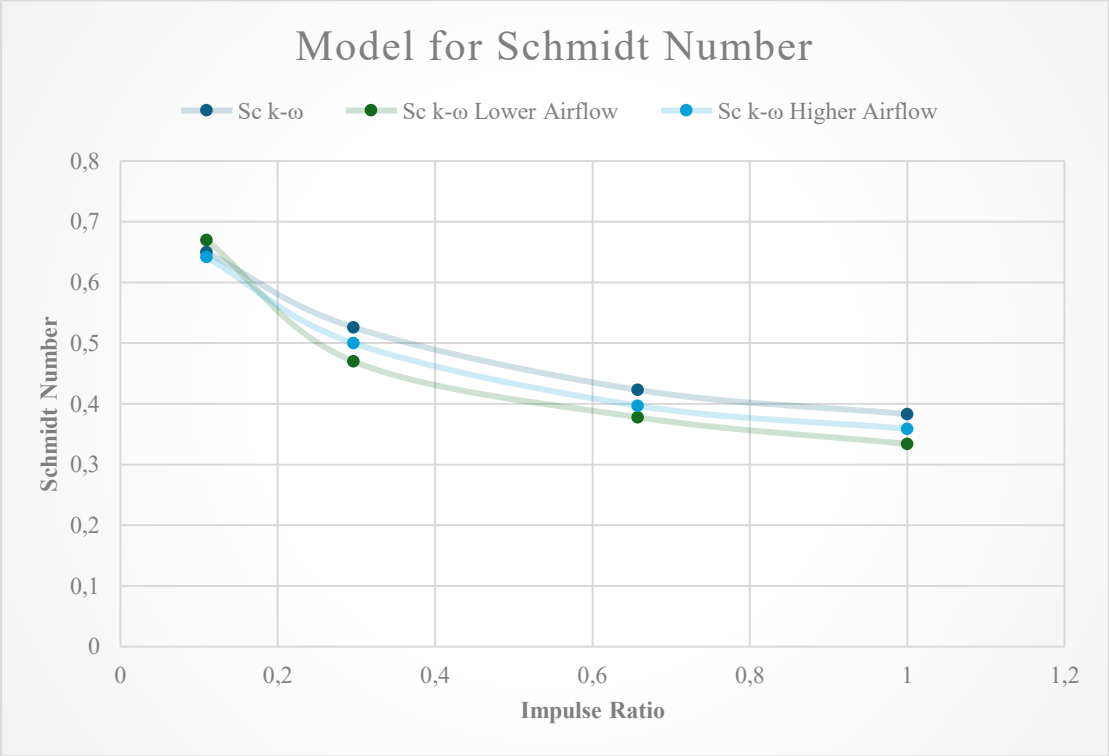

Figure 32 Comparison expanded to different airflows

In the image it is possible to see the choice of Schmidt Number needed to obtain optimal prediction of NO_x production for each condition. For Impulse Ratio higher than 0.2, which are the conditions with $lambda \leq 4.5$, the trends are stable, but for lower value the behaviour becomes less clear, and the model with the lowest inlet air velocity actually needs a higher Schmidt Number correction.

One possible cause could be the lower fuel flow and air flow which are not well predicted by the model irrespective of the Schmidt Number because of the critically small quantity of fuel that has not the ideal penetration in the burner and therefore

mainly attaches to the wall where the turbulence model has less opportunities to predict the right mixing.

Other experimental results for an even lower airflow are available and would probably be able to demonstrate this theory that attempts to explain the anomaly in the trend. In the meantime, the analysis was developed for Impulse Ratios higher than 0.2, where the trend is stable, and results are comparable.

It is interesting to note that the value of the Schmidt Number for a particular Impulse Ratio is not proportional to the airflow, as the highest value belongs to the reference case and not the to the one with the higher airflow. This creates a problem in finding a general solution for the tuning of the model through the analysis of specific parameters: if the Schmidt Number were proportional to the air flow, the tuning of the model in different operating conditions would have been trivial and the predictions would have been easily validated by additional simulations.

It is still possible to find a relationship between the various operating conditions, but it is necessary to develop a theory and demonstrate why the higher Schmidt Number belonged to the reference case for different Impulse Ratios. It would be then necessary to understand how to individuate the point of highest Schmidt Number without experimental data to support the claim.

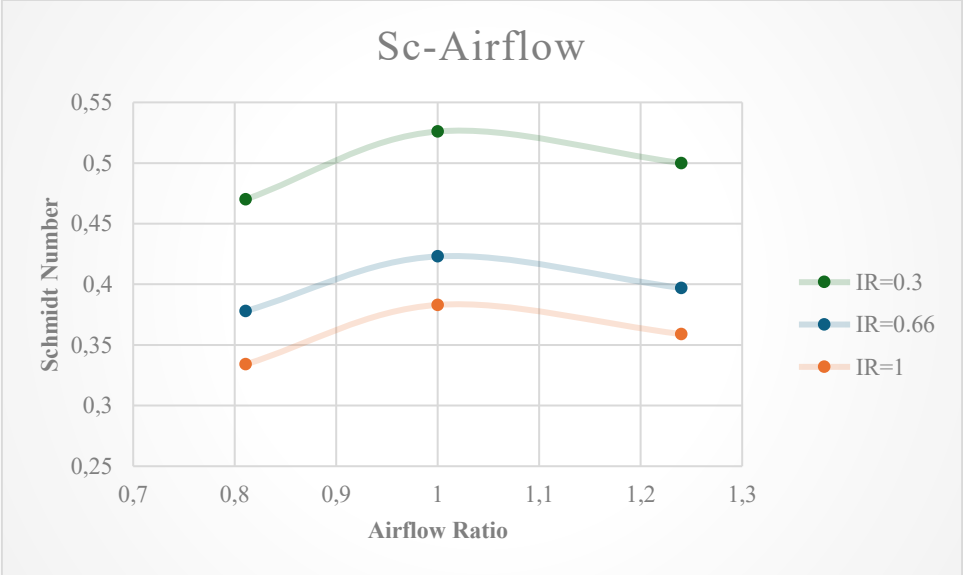

Figure 33 Trend of the necessary setup for stable conditions

The results for IR>0.3, displayed a similar trend for all three different airflows conditions; in this region the tuning could have been possible, but the validity would not be general and the validity for similar operating conditions should have been demonstrated.

It would have been possible to extend the validity of the trend for IR=0.3 if the result for Lower Air Flow were not considered: the same curve could have represented multiple operating points with a simple translation of the function depending on the Impulse Ratio, with the only exception of the only result not in line with this trend that was the result for IR=0.3 of the Lower Air Flow. If this result could have been excluded from the study with the same principle used to exclude the lowest Impulse Ratios for each airflow, a stable trend could have been determined.

It seemed like the model, maintaining the Arrhenius Rate constant and tuning the Schmidt Number, was not the ideal candidate for the prediction of NO_x production for this geometry. The knowledge acquired testing the reference model would also be useful to determine if the differences between various turbulence model could have been considered either a positive or a negative attribute.

The ideal behaviour which was the aim of the study would have been a turbulence model that did not need tuning with different operating conditions or that could be tuned easily thanks to the proportionality between lambda, airflow and Schmidt Number.

5.3.1.2 Transition SST model

Testing the second model, the main focus was to understand the underlining differences in the functioning of the model compared to the reference case. These differences could be of different kinds: the difference in mixing for the same settings, the stability of the model with different fuel flows and the stability with different airflows but similar lambdas. Firstly, the model was run with the same settings of the reference model to be able to do a one-on-one comparison of the main parameters, in particular of the distribution of species, temperature and overall rate of reaction.

The difference of temperatures and turbulence meant that the Transition Model predicted a much higher NO_x production and the results were not comparable. So, it was possible to observe that the tuning of the k-ω model did not work for a model which is essentially an evolution of it, and the other two transport equations evidently have a big influence in the behaviour of the model.

Although the idea behind the comparison with same settings was sound, the big difference in mixing, and therefore reaction and NO_x production, made it really difficult to compare the differences in behaviour of the two model in the mixing zone and a better comparison could have been obtained with the tuned Transition SST model. With the tuned Transition SST model, it was possible to make out which part of the mixing is more influenced by one model compared to the other:

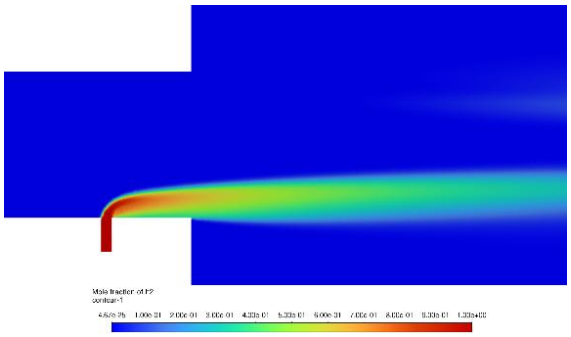

Figure 34 Mole Fraction of H_2 with k-ω SST

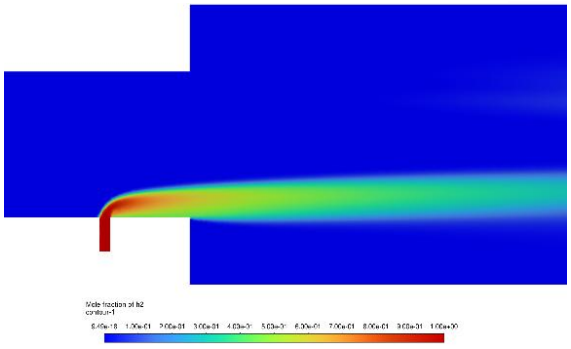

Figure 35 Mole Fraction of H_2 with Transition SST

The two models exhibited a similar behaviour and similar predictions for the base conditions, but small differences could already be derived from the Mole Fraction distribution on the XZ plane.

The first difference could be seen in the immediate vicinities of the fuel injector, where the second model predicts a higher mixing in the zone of higher concentration.

This difference was noticeable for the first part of the mixing until the anchoring point. It was quite visible the faster mixing in the area of higher H_2 concentration in the interior of the flow. The trend is inverted in the later stages of the mixing process, where the k-ω model predicted a wider area of mixing with more expansion in the vertical direction.

The next stage was the comparison of the two models with variable fuel flows, to check the ability of the Transition SST turbulence model to predict the behaviour of the model with higher lambdas and the possible need of tuning.

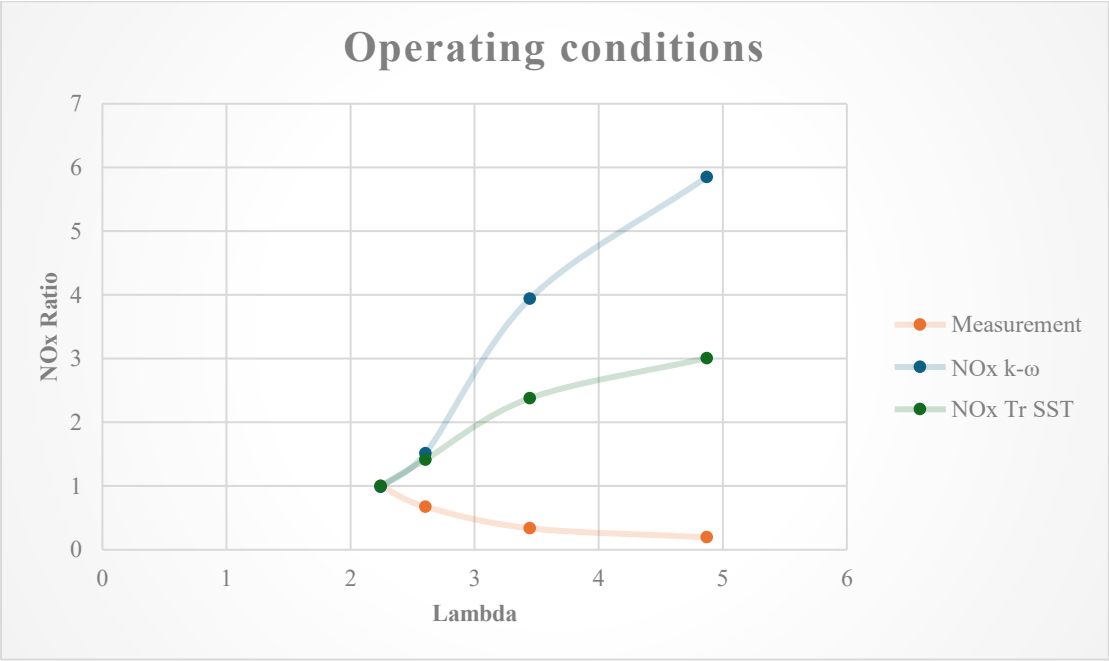

Figure 36 Comparison of prediction capability for the k-ω SST and Transition SST model

Even though the first results seemed to be comparable, with higher lambdas the difference between the two models became starker, with the Transition SST model being able to reduce the effects of wall attachment and instability in the mixing that plagued the reference model. These results could be related to the previous analysis of the different mixing in the two models:

With lower airflow the major difficulty for the models was to correctly predict the separation of the fuel flow from the wall, so the mixing in the first stage gained more importance. The fact that the difference between the two models was not stark could also explain how the Transition SST model was able to deal with lower airflows better, but without being the overall solution for our problem.

The simulations of the Transition model did not represent an ideal behaviour, but the improvement was evident, and it was deemed useful to tune the model for each operating condition, to be able to highlight the trends between this model and the reference.

Predictably, the trend used to find the Schmidt Number that was valid for the k-ω SST was not applicable to the Transition SST model having the same initial conditions, and there needed to be an adaption of the curve to directly relate it to the reference model.

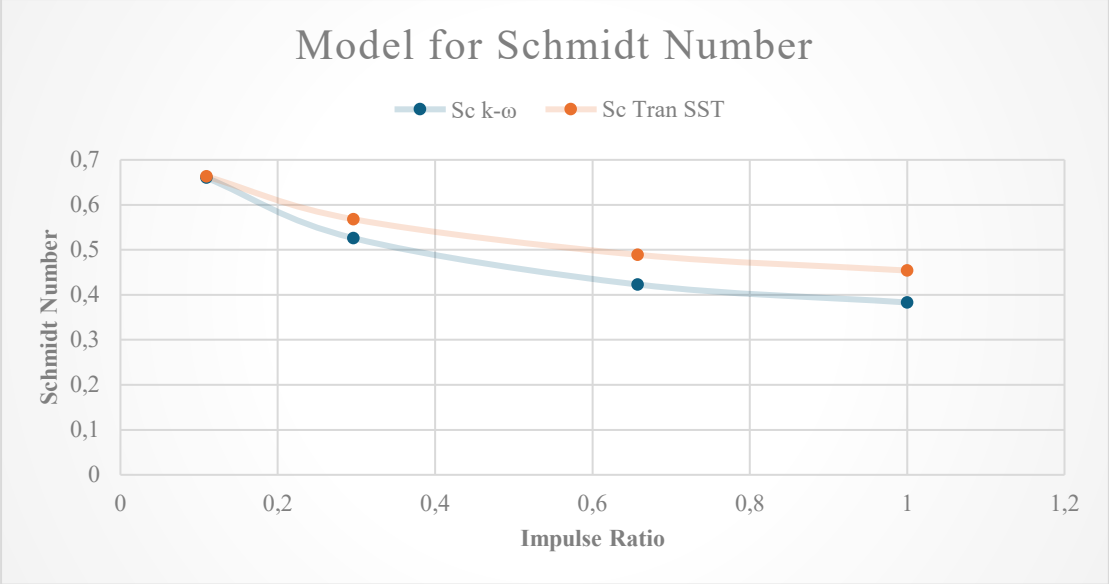

Figure 37 Necessary tuning differences between k-ω SST and Transition SST

For lower airflow, the Schmidt number necessary for the tuning would be the same but the Transition SST model then needed less modifications to give accurate results for higher airflows. These results highlighted a higher stability for the Trans SST model, both for fixed Schmidt Number and for the tuned Schmidt Number, meaning that the model suffered less from perturbation when the operating condition was modified.

These characteristics of the Trans SST model make it a viable option to substitute the reference k-ω model for more stable predictions and lower dependency on external factors, but this model still needs to be tuned for the particular application as much as the k-ω model. Therefore, it is not dependable without tuning and the study proceeded to check if other models could be more effective.

5.3.1.3 RSM BSL

The RSM BSL model has shown that depending on the study, the results obtained could be a big improvement over RANS models or, alternatively, represent an unstable and slower method that does not bring any benefit to the simulation.

Additional research was done in the eventuality that the model would need a calibration of the tensor based on k-ε (Yoder & Orkwis, 2019), or a calibration of RSM ω based (Song, Yu, Liu, & Cheng, 2022), (Praliyev, et al., 2019).

The model did not need a calibration, and it was able to represent the correct behaviour with the default settings, albeit needing to be implemented with the results of a RANS simulation already stored, because otherwise it would have suffered from stability problems and the convergence would have been much slower, if possible at all.

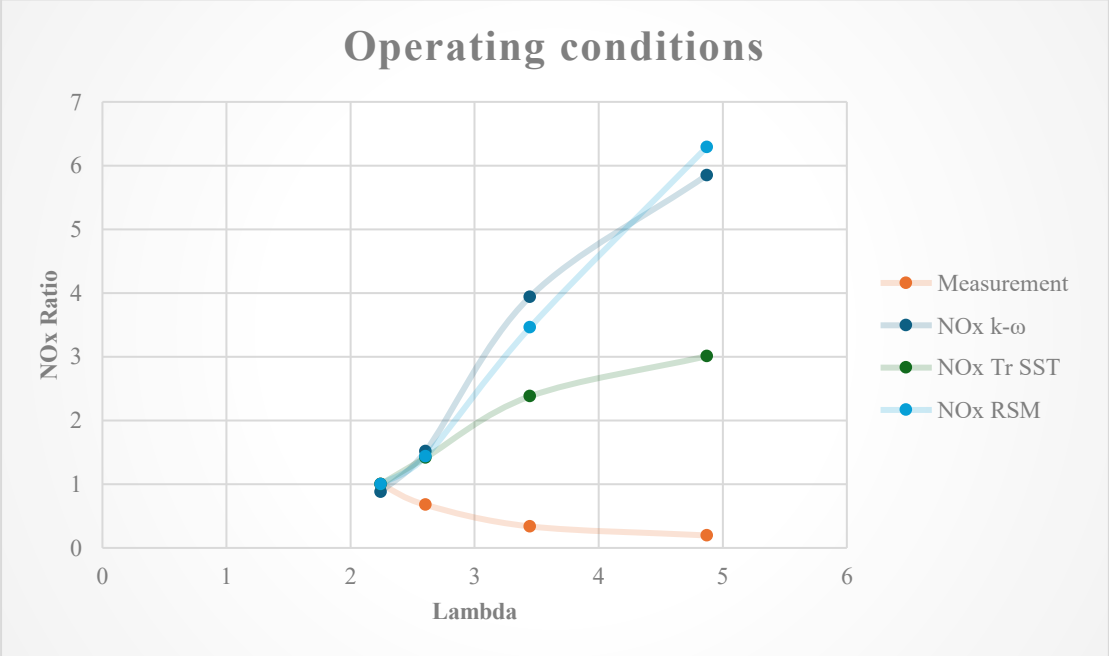

Figure 38 Comparison of prediction capability for the k-ω SST, Transition SST and RSM model

The results were equally as poor as the reference model and in the effort to tune the RSM model to have the same pollution level in the reference operating condition, it was noted that RSM is more susceptible to instabilities with Schmidt Number tuning. All of these results and observations meant that the RSM model would not be suitable for similar applications and the sensitivity to the tuning made it much more difficult to obtain feasible results from.

For all of these models, it was clear how the prediction results degrade once the fuel flow decreases, meaning that the phenomena in the wall vicinity gained importance over the free flow mixing. It was to be demonstrated that the mixing prior to the

attachment of the flow to the wall was well predicted, because limitations of the RANS model could underestimate the impact of the two interacting jets at the fuel nozzle.

5.3.1.4 URANS

Given the instabilities of the k-ω model, it was concluded that also the transient version of the same model would have had the same limitations that were not due to inaccuracies in the transient behaviour, but by the difficulty of the model to predict the right level of mixing for the JICF especially with higher lambdas.

The exclusion of this model was also due to the fact that, these models are capable of sub-par eddies prediction compared to Hybrid RANS/LES and LES models, while still being relatively computationally costly.

The eddy viscosity tensor is shared between RANS and URANS, effectively predicting the same level of turbulence, with the only difference being that the URANS model also contains a term that makes it time dependent.

5.3.1.5 URANS/LES

Of the various hybrid models, the DES (Detached Eddy Simulation) was analysed, and a refined mesh was created so that the areas near the walls would have been modelled with a RANS model and the internal flow would have been directly calculated with LES.

One of the main reasons why the DES was chosen was that there was the possibility to model the near-wall region with various RANS models, and, in particular, it was even possible to use the k-ω SST. This option meant that, using the DES model, the behaviour in the near-wall region would have been theoretically identical to the reference model, meaning that the differences between the LES and k-ω SST in the crossflow region would have been starker and easily noticeable (Menter, 2015).

The first simulations were done choosing a relatively fine mesh and a bigger time-step than it would be advised, and it was mainly done to check the stability of the model and to roughly evaluate the order of magnitude of processing power needed to complete the study of the DES model.

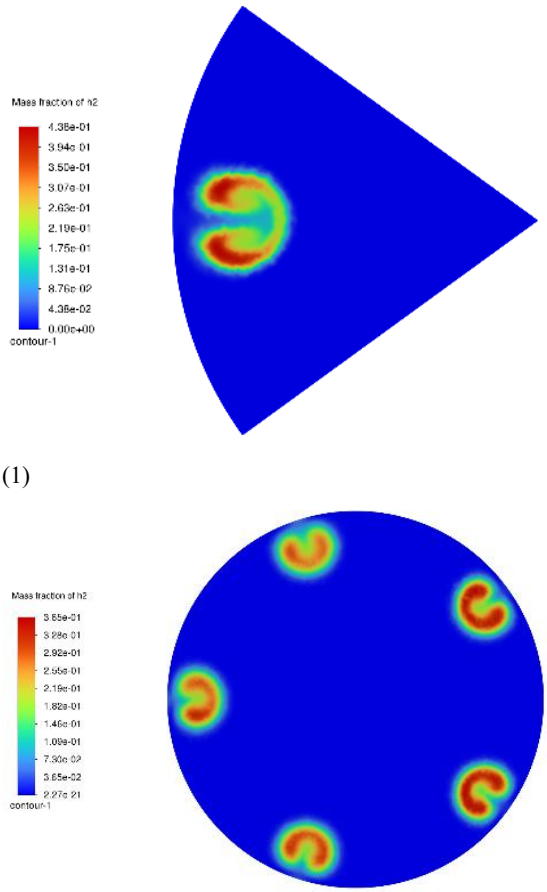

Figure 39 Comparison of mass fraction distribution of hydrogen for the DES model (1) and the reference k-ω SST model (2)

The results immediately revealed the difference between the models in the prediction of the vortices of the crossflow, with the major refinement and direct calculation that enhanced the results of the DES model. It is important to note that, being the DES model a transient model, the results depicted for the DES model are actually the capture of an instantaneous condition which is continuously changing throughout the simulation. This means that the comparison of the mixing through one figure of the H_2 concentration is not as useful as with RANS models.

It was immediately noticeable how much more detail the DES model predicted, approximating the best the counter-rotating vortex formation and from the Figure 39 it is possible to visualize the evolution of the mixing through four time-steps and the semi-unsteady diffusion of H_2 in the mixing zone.

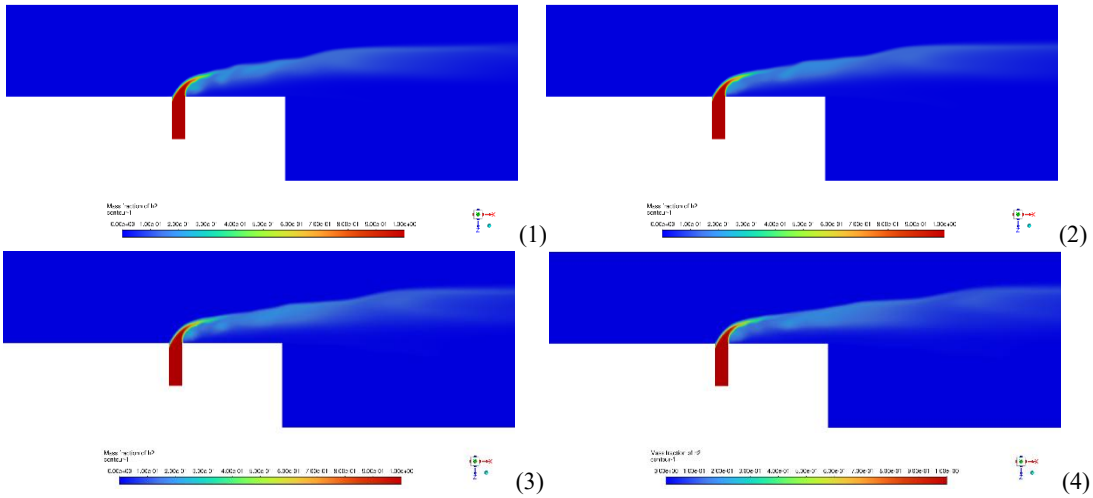

Figure 40 Prediction of the mixing of hydrogen in the crossflow with the DES model

From these captures we were able to understand the principal limitations our model, which displayed an unsteady behaviour only in the free-stream region, but with severe limitations in the prediction of instabilities and turbulence in the fuel nozzle and in the first part of the mixing zone.

It is important to remember that the main reason why the RANS model were deemed as sub-optimal was the struggle of those models to predict correctly the mixing before the anchoring point and the penetration of the jet in the air pipe, so, to understand properly the effect of the LES solver, it was important for the region where the two flows interact to be calculated directly, abandoning the k-ω SST modelling.

Therefore, the DES model revealed to be a useful tool, but inadequate for this geometry where the calculation and prediction of the turbulence in the small fuel inlet made a big difference in the mixing just downstream of it.

5.3.1.6 LES

LES simulations represented a much bigger challenge than regular RANS runs because of the higher computational demand and the higher dependency on the mesh, hence the need to modify the workflow of the testing to try and obtain the best possible predictions.

The simulation was predicted to be much more computationally costly than the previous ones, therefore the strategy to limit the computation time would include firstly the modification of the geometry: the burner was divided into five part each having a fifth of the pipe with one injector in the middle, creating other symmetry faces to account for the inside area of the burner.

The necessary higher refinement meant that reducing the size of the geometry represented a crucial step in the development of a feasibly efficient model.

Another critical point of interest for a LES simulation is its instability when the boundary conditions of the model are not correctly defined, even more so when the simulation involves reacting elements. To solve this problem, it was suggested to develop the inlet flows with separate simulations either with simulations with periodic boundaries or elongating both air and fuel inlets and run independent simulations where only the flow in the pipes was considered.

The velocities for air and fuel could then be exported as velocity profiles that would have then been used with the RANS and LES models to get rid of inlet instability and turbulence variation.

Instabilities in the LES simulations also led to the need of having a set of data and a stable starting point for the LES simulation given by a RANS model, which was used on the same reduced geometry to get close and stable results. Other than the results data, other important parameters were derived from the simulation to help in the sizing of the mesh and the time step for LES.

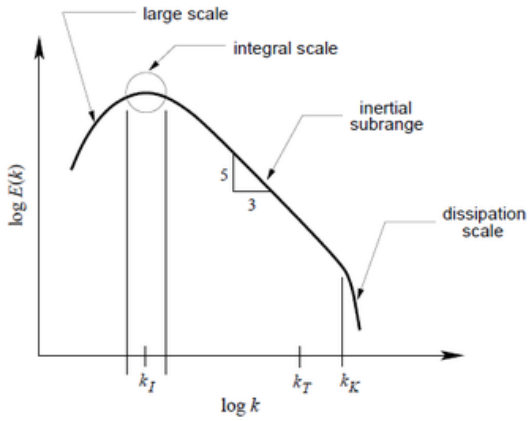

Figure 41 Distribution of turbulent energy in relation to the dimensions of the eddies in the flow

To understand the level of refinement needed for the LES model to calculate the inertial subrange it was first necessary to calculate the integral length scale, a measure of the dimensions of the eddies which carry the most energy.

Setting up a mesh with dimensions four or five times lower than the integral length scale would ensure the correct calculation of all the most important eddies and the RANS predictions were used in the calculation:

$$l_0 = \frac{k^{1.5}}{\varepsilon};$$

(17)

Where k would be the turbulent kinetic energy and ε the dissipation rate of the flow; the mesh having dimensions so that:

$$\Delta \approx \sqrt[3]{Cell\ Volume}, \text{ with}$$

(18)

$$\frac{l_0}{\Delta} = 5;$$

(19)

The latter equations were used to obtain a mesh refinement that would be able to solve approximately 80% of the eddies. This choice was considered a good compromise between precision and computability, also considering that this would have been the first attempt with the new model and there was a chance that the model would have needed significant setup modifications to reach an accurate prediction.

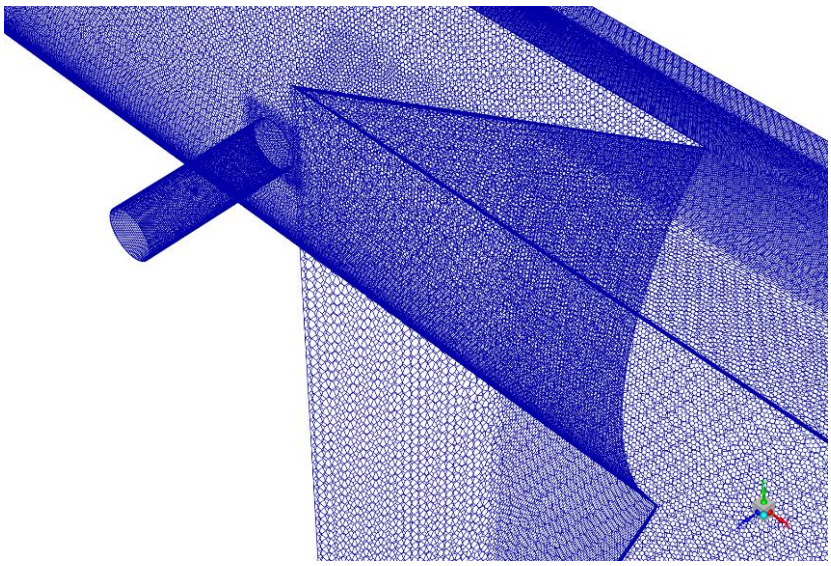

Figure 42 Detail of the Mesh refinement around the fuel inlet

Initially, there was a problem with Fluent which could not recognize the data from the RANS simulation because of a difference in the size of the time step between the two models, creating the need for a new simulation with the URANS model, set up with the same time step as the LES one.

The difference in mesh probably limited the possibility of loading the stable results on the LES model, and adapting the mesh to run with the k-ω model did not guarantee the

problem to be solved, so, once every boundary was well defined the simulation without combustion was started, to check if the flows could be predicted with the starting mesh.

The first simulation did not yield stable results, and while studying the case the cause of these instabilities was clearly defined as the refinement of the fuel pipe, which exhibited strong gradient in velocity and temperature. This kind of instabilities was widely reported by the literature, most probably caused by the lack of refinement in the wall region where the model struggles to predict the smaller eddies.

The inlets were further defined with new profiles that included the velocity magnitude, the turbulent kinetic energy and the turbulent dissipation rate. These parameters, combined with temperature and mixture fractions, meant that the inlet boundary conditions were totally defined, and the simulation should have not suffered from instabilities due to them.

The problems of data transferring between the URANS model and the LES model persisted and the priority was set to resolve this issue as the LES model would have been even more unstable and computationally heavy than what was predicted. It seemed like the URANS model did not influence in the slightest the behaviour of the RANS model, and the data of this model, with the right time step size set up, was not readable by the LES model to start the simulation with a stable solution.

This problem was solved with the use of a RANS model on a coarser mesh and interpolating the results once the solution was stabilized. This method did not need the same geometry to transfer the data, but only the same case, given that the program defined a binary code where all the information regarding every cell was stored, such as the velocities, temperature, mass fraction and pressure.

In this way we were able to transfer the data to the LES simulation and to gain a stable starting point for the simulation, with the only limitation that the major difference in cell size meant that the distribution of the quantities in the new mesh could vary slightly with the Rate of Reaction probably having the worse approximation.

Regarding the mesh, difficulties rose when it was time to define the newly obtained internal boundaries as periodic: the main limitation was given by the volume that was previously created to define the area of refinement in the complete RANS model. FLUENT had issues applying the Shared Topology to this volume and sometimes even struggling to generate the surface mesh if the Shared Topology was applied directly in the CAD design.

To solve this problem, a local refinement was manually developed in the same region to eliminate the need for a second body that created many issues in the meshing of an already complicated model. The final model presented a base refinement in all the fluid region, with additional refinements along the air and fuel pipes and the bigger local refinement region where all of the mixing and reactions occur.

The unstable and complicated nature of LES simulation meant that every setting had to be optimized before starting the simulation and it was less advisable to rely on the default settings of Ansys FLUENT.

The case was analysed and compared to the ones present in the literature to understand which modifications would have been more useful and what was the reason behind the choice of any of them. One of the first choices to be made was the one of the Sub-Grid Scale (SGS), which defines the model behaviour for eddies that cannot be solved directly by LES.

The SGS chosen was the Dynamic TKE SGS, that was considered the most suitable for several reasons, the more important being its ability to deal with reacting flows and the possibility to visualize which part of the model is resolved directly by LES and which one is modelled through the SGS.

Another need of the model was to have fully developed boundary conditions to prevent instabilities in the pipes, and for this reason the default settings of "No Perturbations" was considered, as well as of the "Synthetic Turbulence Generator" which was set up using the turbulence profile obtained from the study of the fully developed inlets.

The choice of the Dynamic TKE model was corroborated by the fact that this SGS model, according to the literature (Gerasimov, 2016), worked the best in dealing with the synthetic turbulence generated at the inlets. The outlet was not modified in this way as the only requirements on it was that it was important not to have backflow to be able to measure variables at the outlet with accuracy. The backflow, as explained in previous passages, was eliminated with the use of a sufficiently long burner, which made the model computationally heavier but had a positive impact on the precision of the predictions.

Following the suggestions found in the CFD literature, the time-step was set from the condition of:

$$CFL \leq 1 \tag{20}$$

Where CFL is the Courant-Friedrichs-Lewy number, which is defined as

$$CFL = \frac{v \cdot \Delta t}{\Delta x} \tag{21}$$

with v defining the flow velocity, Δt the step size and Δx the grid resolution.

The strategy implemented was to prioritise stability at the beginning of the simulation and then focus on faster convergence once stability was optimised; that meant that the number of iterations was increased for the first time-steps, while, after the stability had

been properly addressed, a bigger time-step size and a lower number of iterations per time-step were considered.

The first simulation was developed and, even though FLUENT did not encounter a critical issue during the simulation, a warning was issued that signalled the malfunctioning of the Synthetic Turbulence Generator at the inlets, apparently due to the turbulent length scale, which could not be represented through the chosen mesh.

The turbulent length scale is a physical quantity that defines the size of the large eddies that contain most of the energy, and it was defined as:

$$l = 0.038\, d_h \tag{22}$$

Where d_h for a pipe is the Hydraulic Diameter.

This simple formula was used to determine the level of refinement needed for the inlets and the modifications were limited to the fuel inlet where the mesh did not respect the requirements. The refinement volume was created to include only the inlet fuel and reduce the cell size to respect Equation (22). Different settings were considered, when it came to the turbulence parameters to be specified, and the final choice were the profile of the turbulent energy k and the one of the dissipation rate ε.

The reasoning behind the first implementation of the "No Perturbations" model, was the fact that the turbulent eddies in the inlet fuel were relatively less important for our study compared to the ones created in the crossflow. Unfortunately, this model proved to be ineffective in reproduce the air profile in the fuel inlet, with peaks of velocity in the boundary layers, with much less velocity in the middle of the jet.

The first simulation with the Synthetic Generator was also done without the implementation of the combustion, abstaining from defining the species of the fuel, so that we would have had a simpler and more precise definition of the interaction of the flows and the general behaviour of the turbulent flow. A criticality was found on the air pipe where the mesh did not satisfy the requirement of $y^+ \leq 1$ and the boundary layer was modified to have better prediction there.

It is important to stress that the model created for the LES simulations was much heavier than any of the RANS models, therefore it was imperative to modify and refine the model only if strictly necessary and the model was developed following this principle, always considering that the implementation of different ideal settings would have rendered the model a non-viable option.

It is also critical to remember how the solution in a LES simulation is time-dependent and contours and path lines of the last iteration could not describe by themselves the stable solution. The instantaneous results after one thousand iterations were analysed, but not many conclusions could be derived from it, other than the observation that the flow behaviour is clearly different from the one found with RANS simulations.

Further development was needed to make sure that the model was storing all the necessary data at each time step, so that the trend of the whole flowtime could be included in the study. The process was streamlined to avoid the creation of a full data file for each step, but it still represented a great quantity of data, so another strategy was developed in parallel. This strategy consisted in the creation of pictures of post-processing for each time-step without the need for the data file to be processed and that meant that, for longer simulations, the data files would not be a limiting factor anymore.

The second simulation was developed also considering the combustion, checking every few time-steps if the combustion rendered the model unstable, but it was not the case, and the choice to introduce combustion from the beginning cut a sizeable amount of time from the simulation.

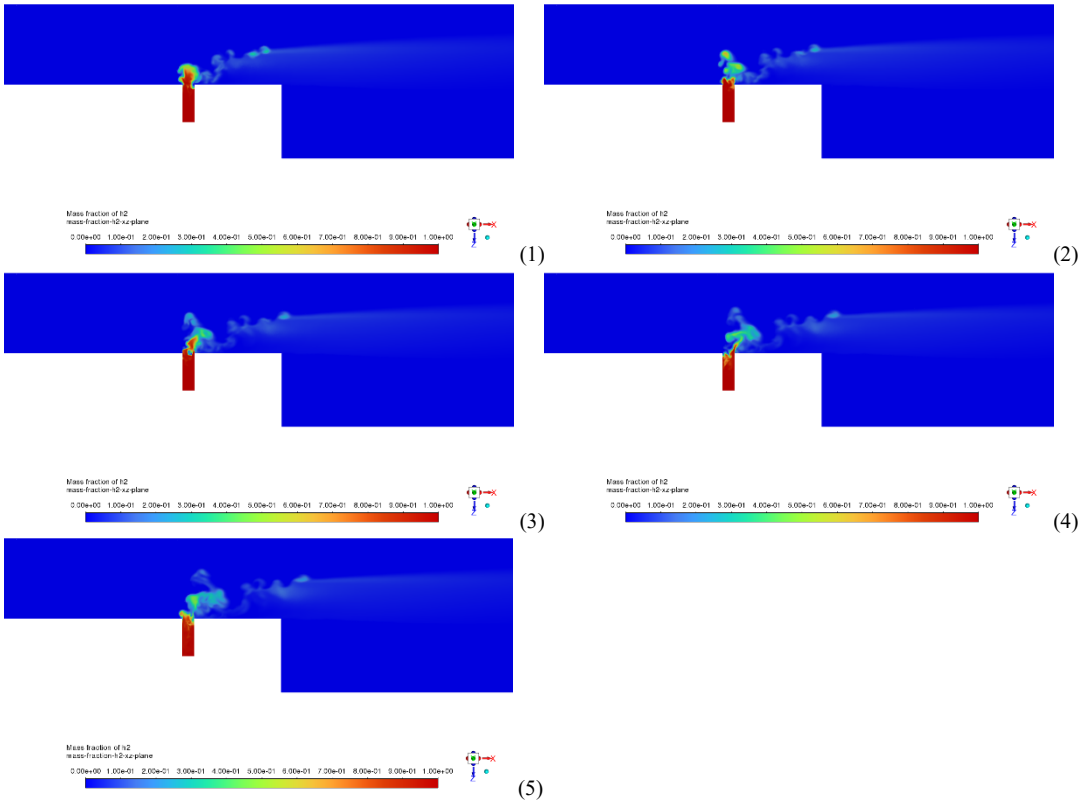

Figure 43 Progression of the diffusion of H_2 in the burner

The period between these images is of ten time-steps and they were useful to appreciate the instabilities of the LES that are predicted through the direct calculation of the turbulent flow. It is evident that the flowtime considered was not enough to completely define the flow and the first estimation was that around ten times the amount covered up to that point would have been able to describe the major characteristic of the flow adequately well.

There were initial doubts about the stability of the model because temperatures and heat produced were dropping, but instead of stopping the simulation and correct the inaccuracy with a virtual heat source, it was deemed preferable to leave the calculation going to, at the very least, have as a starting point a fully developed LES flow.

The strategy to analyse the LES model results consisted in various points of discussion that would have been studied independently. Starting upstream, the first comparison would have been the velocity and turbulent study of the inlets, to check if they presented singularities and if the predictions were comparable with the RANS models.

The next important step would have been the analysis of the mixing, both right around the nozzle and downstream of the anchoring point, with great attention to the mixing rate and mixing zone location compared to the wall. The reaction would have been a consequence of these parameters, and its behaviour would have had to be compared to RANS simulations, in particular the peaks, length and stability of the reaction.

5.3.1.6.1 Post Processing and Results LES

Inlets

As mentioned above, the strategies used to define the inlets for the two model were different, and the behaviours of the inlets reflected that: the RANS model worked with the “flat inlets” and without any specification of turbulence, while the whole definition of the inlets of the LES was necessary to give the model the starting point for the turbulence prediction, but it also introduced new possible causes of instability and uncertainty.

The turbulence of the fuel inlet, in particular, revealed to be quite difficult to properly define and the flow was firstly deemed unfeasible because of the great difference in velocities of the inlet flow of the two models. The difference was stark, but the mass flow rate was checked for both models and the two values were almost identical, therefore, even though the instantaneous value could vary timestep after timestep, it was considered that both models were representing the true behaviour with different levels of precision.

Figure 44 Turbulence singularity at the fuel inlet at the start of the simulation

Mixing

Four parallel planes were created both in the RANS (odd numbers) and LES (even numbers) model to record the pattern of mixing along the X axis of the model, in the first instances after the entrance of the jet fuel crossflow.

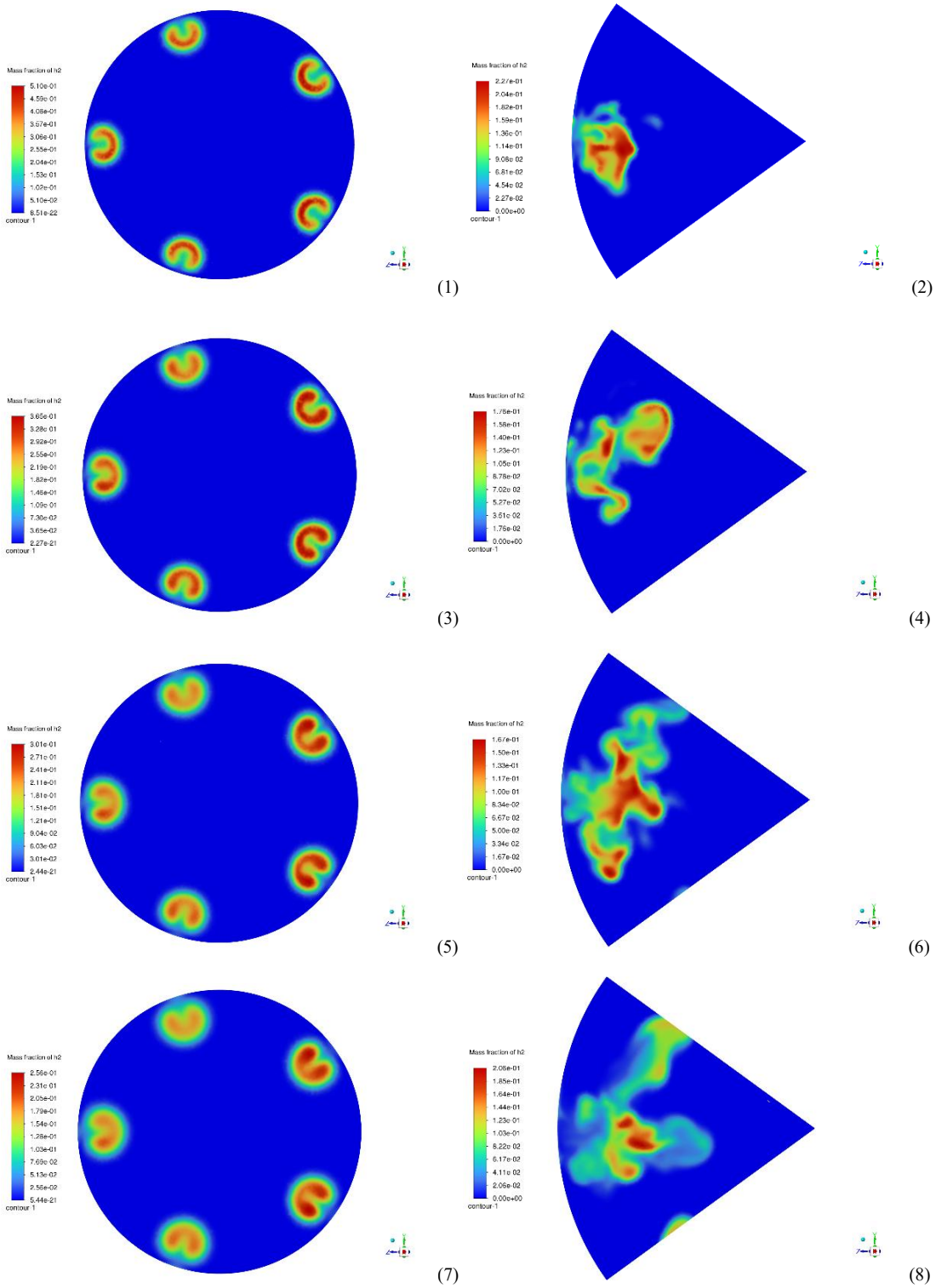

Figure 45 Hydrogen distribution for RANS model (odd) and LES model (even)

Even though the images were taken from a timestep that does not represent the fully unsteady flow, they were considered interesting to analyse because the LES flow was already developed in the mixing zone and the trend present was then confirmed again by the subsequent time-steps.

The first observation was that the concentration of hydrogen on all the planes highly differed between the two models with the LES model corroborating the notion from the literature that the RANS models overestimate the eddy viscosity of the flow, therefore underestimating the mixing. That alone was a big limiting factor in the prediction of turbulence flows, especially reacting ones where the mixing is the most important phase.

Furthermore, it was noticeable that, while the RANS model predicted stable counterrotating vortices, the LES model did not, but, given the behaviour of the mixing on the other plane, it was fair to assume that the dynamic solution of various time-steps would have approximated these vortices much better, as mentioned by (Nair, et al., 2019).

The concentration of H_2 decreased steadily throughout the recording planes in the RANS simulation and that was not the case for the LES, in particular it was noticeable how the distribution and mixing of the hydrogen happened in waves, with pockets of hydrogen which detached periodically from the inlet flow increasing the mixing surface and speeding up the diffusion. That meant that the concentration had recurrent peaks throughout the planes, with a periodicity that could have been calculated once the flow was fully developed.

It was also possible to visualize the development of the turbulence at the fuel inlet creating an Iso-Surface with constant “Q Criterion Raw”, which helped in visualizing the vortices created by the crossflow and in appreciating how the interaction between these vortices enhanced the mixing.

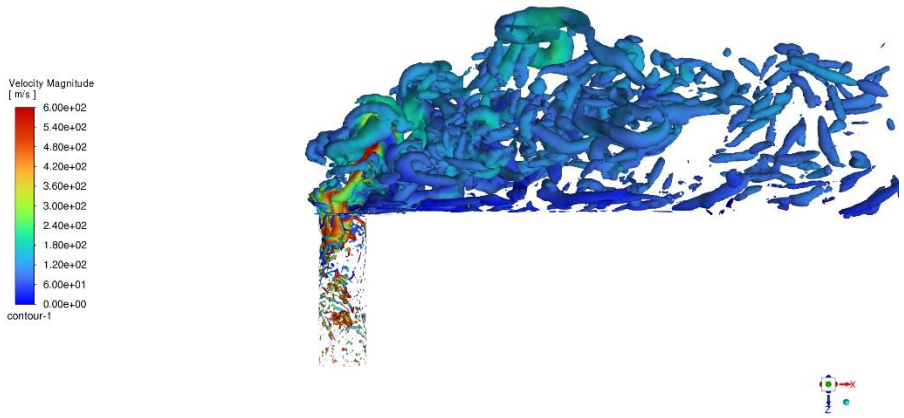

Figure 46 Crossflow turbulence

Combustion

While the Instantaneous Static Temperature showed a completely different behaviour to the one obtained with RANS, the Mean Static Temperature showed how the average trend of temperature for the LES model was much more similar when the instantaneous peaks of temperature are not taken into account.

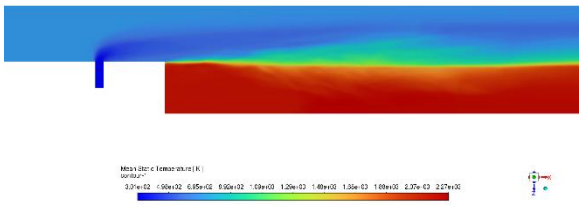

Figure 47 Mean Static Temperature LES

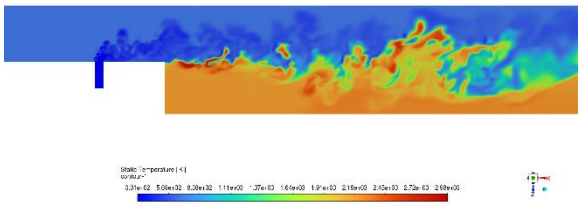

Figure 48 Instantaneous Static Temperature LES

The ignition of the combustion was stable and immediately downstream of the anchoring point. The peak in temperature in the instantaneous contour could have caused higher emissions of NO_x compared to the ones predicted by the average contour.

The model would have needed to be properly tuned to be compared with the RANS model and to understand if the faster mixing would have been enough to offset the peaks of temperature.

Through the recording and analysis of the Unsteady Statistics, it was possible to obtain more information on the model:

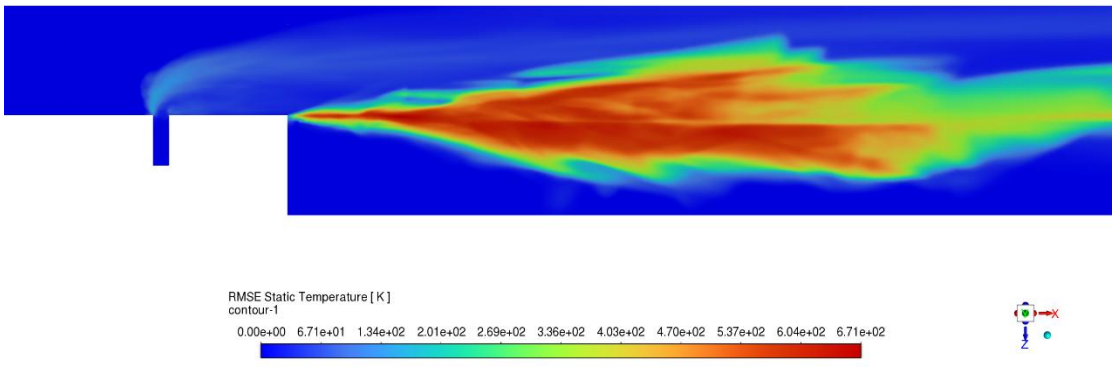

Figure 49 RMSE Static Temperature LES

From the RMSE Static Temperature in Figure 49 it was possible to appreciate the areas where there was a higher variance in Static Temperature throughout the time-steps. The oscillatory behaviour of the flame is clearly visible where the variance is higher, meaning that those regions were part of the flame in certain time-steps, but part of the surrounding flow in others.

Furthermore, as mentioned earlier, the implementation of the SGS model "Dynamic Kinetic Energy" meant that the Sub-Grid Kinetic Energy could be obtained directly

and, therefore, the percentage of turbulence resolved would be easily calculated. This quantity was defined as:

$$Resolved\% = \frac{Resolved\_k}{(Resolved\_k + SubGrid\ Kin\ Energy)}, \text{ with}$$

(23)

$$Resolved\_k = \frac{1}{2}(rms_{x_{vel}}{}^2 + rms_{y_{vel}}{}^2 + rms_{z_{vel}}{}^2)$$

(24)

being the kinetic energy directly resolved by the LES model. The results were close to the expectations, with a complete resolution away from the wall and crossflow, and with good resolution in the mixing zone, where only the dissipating smaller eddies were resolved with a combination of modelling and direct solving.

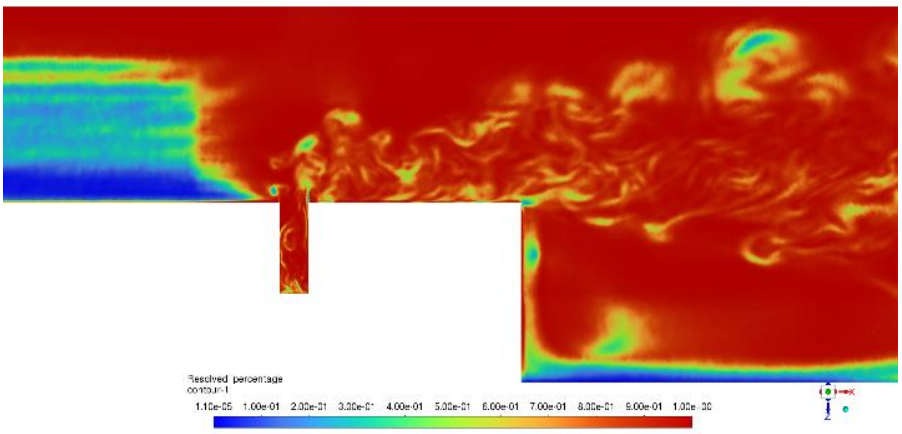

Emissions

Unfortunately, the simulation was stopped before it was possible to complete the flush-out of the RANS solution that was used to initialize the simulation; that meant that the pollutants recorded at the outlet still belonged to the RANS model and not to the LES. So, although the combustion was completely defined by the LES model, the only results that could be derived were regarding the maximum temperature and the visual study of the development of the combustion in the chamber. The NO_x pollutants are more concentrated in the vicinities of the peaks of Rate of Reaction, and it is probably a consequence of the highest level of turbulence that limits the development of a hot zone.

5.3.2 Combustion Model Variation

Most of the study has been conducted utilizing this model and giving greater attention to the possibilities related to the use of different turbulence models. It was evident that the motivation behind this change of plans was due to the results of the first simulations, which highlighted the high dependence of the model on the mixing and, therefore, on the turbulence models. For these reasons, the study of the various combustion models was delayed and then relegated to the testing with only the reference turbulence model k-ω SST.

The research of the literature highlighted how the various combustion models might have needed for a specific Arrhenius rate for each model, maintaining all the other parameters unvaried. This meant that the comparability between the models was greatly reduced, and the choice of the combustion models would have needed to be analysed on a case-by-case scenario.

The first model tested apart from the reference Eddy Dissipation-Finite Rate was the simpler Eddy Dissipation Model.

5.3.2.1 EDM

The model represents a simplification of the reference combustion model ED/FR, and it theoretically should represent the same behaviour without the damping brought by the finite-rate condition. The reduced geometry from the LES simulation was used, a coarser mesh was developed both for simplicity and efficiency, and, after being set-up for a steady-state simulation with the k-ω SST model, the EDM model was selected.

The results of the simulation highlighted the difference between the two models, as the EDM had an unstable behaviour with the start of the combustion being upstream of the anchoring point, which were similar results to (Ayed A. H., et al., 2015).

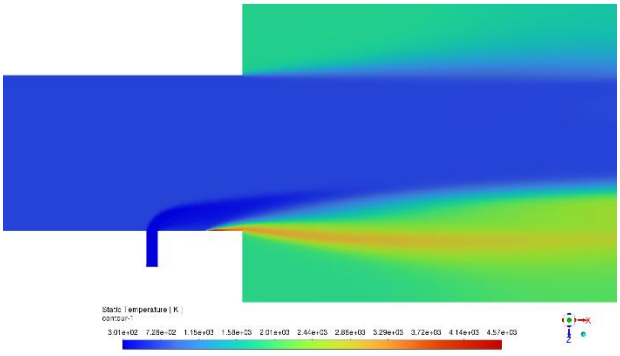

Figure 50 Static Temperature with EDM model

The turbulence was not affected at the fuel nozzle and the initial mixing was comparable, but the onset of the combustion earlier than the anchoring point also modified the flow downstream obtaining a behaviour that was different from the reference case. The early combustion was justified by the fact that the reaction was not limited by the theoretical finite-rate of the chemical reaction, and it only depended on the speed of the mixing. This meant that the use of this model would not be suitable for geometries and applications where the mixing and the reaction rate are not in the same order of magnitude, resulting in an early or late ignition, depending on which one of the rates is prevalent.

5.3.2.2 EDC

The EDC model was selected maintaining all the other specifications constant to create the most generally applicable study on its distinctive characteristics. Compared to the reference model and the EDM, the EDC model displayed instabilities that needed to be addressed to run the model properly. In particular, the major issue was the error "dasac failure" at a particular temperature that occurred for every iteration, meaning that the solver was not able to find a suitable solution with that specific temperature.

This problem was already noticed in the preliminary runs and different strategies were tested to solve it; the first was the stabilization of the solution through prior convergence with a simpler combustion model and then with a final simulation with the EDC model (Cheng, Zong, & Zhu, 2024), the second was the refinement of the mesh in the areas of higher interest for the model and the third was the tuning of the Arrhenius Rate.

To make sure that the results could be comparable with the other models the third option was promptly discarded, and both other strategies were implemented. The error was solved, and the post-processing was developed to understand the behaviour of the model, being the numerical results of pressures, temperatures and emissions all comparable or identical to the reference case.

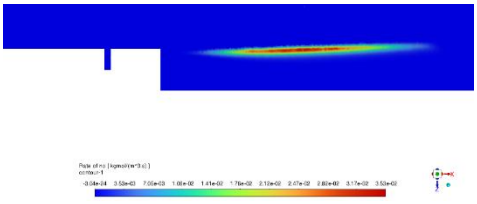

Figure 51 NO_x rate EDC model

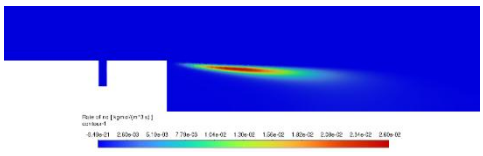

Figure 52 NO_x rate ED/FR model

The rate of production of NO_x displayed a different trajectory of the flame, that was parallel to the axis of the burner for the EDC model and angled towards the wall of the combustor in the reference case.

It was also noticeable how the reaction in the EDC model started later while being more elongated, both the observations leading to the conclusion that the reaction in the EDC model could have been slower, both in the activation and throughout.

A similar analysis was conducted to study the mixing and distribution of H_2 downstream of the inlet.

These contours confirmed the hypothesis previously mentioned and the comparison of the two model showed the slightly slower mixing of the EDC model, which has a higher concentration of H_2 at the beginning of the crossflow and it maintains it evolving towards the outlet.

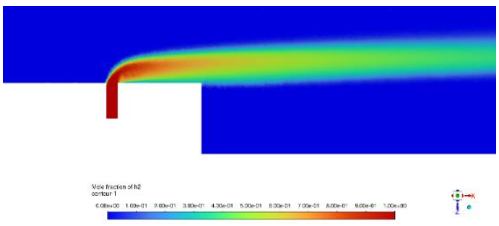

Figure 53 Mole Fraction of H_2 In the EDC model

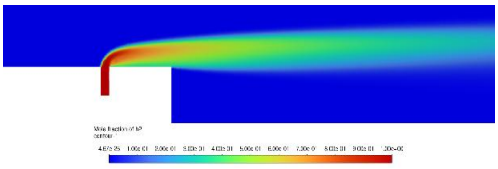

Figure 54 Mole Fraction of H_2 in the ED/FR model

It is also visible from this perspective how the higher concentration of H_2 at the anchoring point in the EDC causes the prediction of the flow to be more streamlined and to not be affected by the anchoring point as much as the reference model.

5.3.2.3 PDF Flamelet models

The last combustion was the one that was widely regarded as the best alternative to the standard ED/FR model, and it needed some additional setup compared to all the Eddy Dissipation model. To implement it, it was needed to develop both a Flame Function and a PDF Table and the kinetic mechanism H2_mech was used as input to create both.

The results of the simulation were not in line with the previous models, which have some variance, but the same general behaviour, and displayed a much higher reactivity also compared to the EDM that had no damping coefficient.

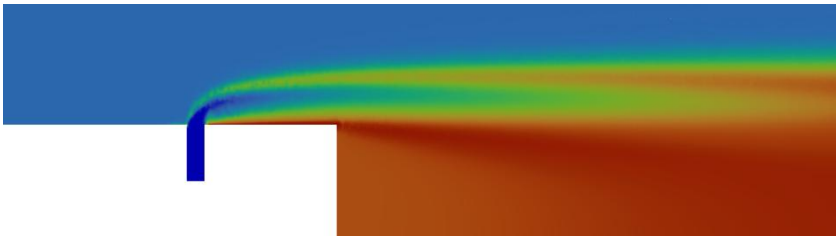

Figure 55 Static Temperature PDF model

As it can be seen from the contour that describes the Static Temperature, this model predicted an even earlier onset of combustion right at point of interaction of the two flows, upstream of the main inlet output. This meant that the model predicted instantaneous ignition of the mixture, with no limitations of activation energy and the mass concentration of the two elements.

This behaviour was obviously considered sub-optimal and the mole fraction contour confirmed that the high temperatures shown in the Figure 55 were not due to the recirculation of hot gases back into the air pipe.

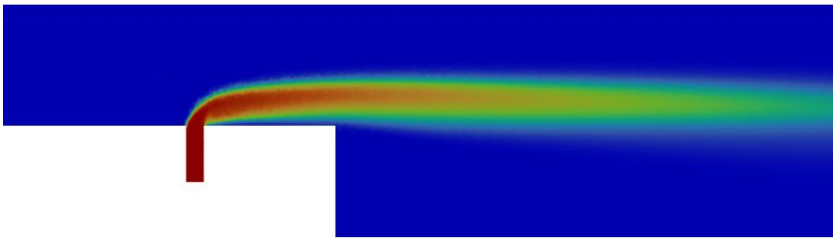

Figure 56 Mole Fraction of H_2 with the PDF model

It can be seen that the region between the area of higher hydrogen concentration and the wall, the concentration decreased slowly, meaning that the combustion developed from the wall and the high temperatures were not due to flashback of exhaust gases that would have otherwise limited the diffusion of hydrogen in that region. It was also unfeasible to theorize that the flashback could have extended even further upstream that the injector itself, confirming that the model was grossly overestimating the reactivity of the flow and that it was in need of a major tune up.

It is important to make an observation on the simplicity of the set-up of said model and on the stability of the solution that, even being not physically representative, was reached in a reduced number of iterations and it would with all probability be important to consider if the model was to be tuned and used in the future.

6 CONCLUSIONS

The results of the different models and the development of different mesh were useful to gain an understanding of the Turbulence and Combustion models behaviour, but also to understand strengths and limitations of the burner concept. The critical areas of interest that were the most difficult to deal with were the fuel inlet and the first area of mixing right at the point where the two flows interact. The prediction was, as stated, affected by the mixing more than by the combustion. That meant that the study of the turbulence models gained more importance compared to the combustion models and relative differences between turbulence models would have had a bigger impact on the study than the combustion ones.

RANS models are considered a good compromise and that is why they represent the most popular option for a lot of application in the industry sector. They showed optimal stability and for the particular micro-mix application, they also had great accuracy in the prediction of the generation of two of the crossflow vortices, the horseshoe and the counter-rotating vortices. Their limitation stood in the poor prediction of the leading edge and lee-side vortices, which meant that all of these models would have a poor mixing prediction in the first phase of diffusion, leading to slower mixing and to a heightened wall sensitivity because of the slow mixing. The variability of the results for different operating conditions made these models undesirable for the current studies and for the design of new geometries that have not been experimentally tested and, therefore, have no data to reach the correlation needed to tune the RANS models.

It's important to note that the conclusions reached testing the k-ω SST model were extended to other two equations models thanks to limited preliminary testing on the k-ε realizable model and to the incredibly vast collection of literature that confirmed the k-ω SST model to be the most suitable model for this application, with a superior near-wall prediction compared to the rest. This model was then integrated into the Transition SST model, which comprises of four transport equations and showed improvements in the critical areas compare to the reference model. The model achieved a better prediction in the first part of the mixing zone, resulting in a much better stability throughout the different operating conditions, while, even if it should have been theoretically slower, the difference in computation time was negligible.

If future research and studies on the topic were to be limited by computational power, this model would most probably be the recommended one, as it strikes the best compromise between lightness and stability, both on its dependence on different conditions and on different tuning settings.

The simulations with the RSM BSL model confirmed the information already available about this model (Yilmaz, Cam, Tangoz, & Yilmaz, 2017) as it showed to be easily affected by change of tuning and conditions. This means that, at least for current

applications, it is difficult to understand how the model would behave with a different geometry. The Reynold Stresses Model was less stable than the previous models with different operating conditions and it needed a higher level of refinement for the tuning, meaning that it was heavily affected by small changes both in the setup and tuning.

Furthermore, the model was deemed to be not suitable for the current geometry and similar designs as the results were not offering any improvements on precision, while being sensibly slower in the calculation.

The DES model was the one that showed the most potential, not for this geometry, but for general industrial applications of CFD studies and the reasons why are of various nature. The first would be the fact that, considering the advancements in technology of the last years, it is fair to assume that the model would be more appreciated once the computational weight will be less relevant in its implementation. Another advantage of this model is its flexibility, as it can be used to obtain LES precision in the areas of interest while the stability of the other areas is guaranteed by the RANS model instead of a near-wall function as in the LES model. Depending on the need, the model is capable of obtaining different levels of precision, with the choice of the appropriate mesh refinement and dimension of the Time-Step.

The problem behind the underutilization of this model in our study was the fact that it was not really compatible with the selected geometry, as the turbulence in the fuel inlet and in its immediate vicinities was crucial to the behaviour of the flow and the RANS model was not suitable to predict them, but a further refinement of the area would have resulted in a simulation that resembled in every way the LES model, losing the computational advantage and stability of the DES model. The problem was that, being that area so important for the correct prediction of behaviour of the entire combustor, there wouldn’t have been a good compromise between precision and computation time, either being too close to RANS and having trouble predicting the correct flows or, as mentioned before, being close to a full LES model, but having lower accuracy and a still considerably large computational weight.

The LES model, as much as the RSM, confirmed the initial reports from the literature, it being by far the most precise and the heaviest model. The big difference between LES and RANS model was in the ability of the former to correctly predict the onset of the leading edge and lee-side vortices, considerably increasing the interacting surfaces in the first part of the mixing and, therefore, the near-field mixing is enhanced. This means that the LES should be able to deal with lower fuel and air flows much better than the other models, effectively eliminating the wall attachment phenomenon that caused instability in RANS models. The limitation of LES, as previously mentioned, has always been in the sheer size of the simulation and to the fact that, given the need of small Time-Step size, to obtain a solution for a sizeable amount of time, the number of time-steps needed would be really high.

The comparison of the combustion models analysed was not possible because, for each one of the models run with the same setup, the behaviour was completely different. In particular, the big difference consisted in the moment in which the reaction started and no one but the reference model had the reaction starting at the anchoring point.

The EDM is similar to the reference model ED/FR, but it is not limited by the same chemistry equation, therefore if the turbulence was enough for a flammable mixture to be formed, then the reaction would be able to start before the anchoring point, as happened in the case of our geometry.

The EDC was widely regarded as a good alternative to the reference model, but it was found to be more difficult to setup and the stability of the final solution did not reflect the stability of the model in its entirety. It also underestimated the combustion compared to the ED/FR, needed a finer mesh and a stable solution with the reference had to be loaded to start the simulation.

The Flamelet model had a similar behaviour to the EDM model, with an incredibly early ignition that meant that the reaction started as soon as the two flows came in contact with each other. The consequence was a completely different behaviour that was not in any way comparable to the reference model and, although various sources seemed to agree that the model would have had a stable behaviour, the reality for the particular setup was different and the study of the model was inconclusive.

For a lack of time, it was not possible to complete the analysis of the LES model from the point of view of the emissions, because the model would have needed to run long enough to completely flush out the RANS solution, but given that the previous analysis of the other models gave a good picture of the characteristics needed for the turbulence model to be stable and accurate in every operating condition, it was concluded that the model represented a good solution to solve the problem previously stated.

The combination of a stable combustion model like EDC with different turbulence models could balance out the instability due to the different operating conditions and it would be interesting to research more on the topic.

It is also considered that further studies on the applicability and stability of the DES model could lead to interesting results and to a much deeper understanding of the characteristics of the two models of which it is composed.

7 REFERENCES

Ayed, A. H. (2017). *Numerical Characterization and Development of the Dry Low NOx High Hydrogen Content Fuel Micromix Combustion for Gas Turbine Applications.*

Ayed, A. H., Kusterer, K., Funke, H.-W., Keinz, J., & Bohn, D. (2017). CFD based exploration of the dry-low-NOx hydrogen micromix combustion technology at increased energy densities. *Propulsion and Power Research 6*, 15-24.

Ayed, A. H., Kusterer, K., Funke, H.-W., Keinz, J., Striegan, C., & Bohn, D. (2015). Experimental and numerical investigations of the dry-low-NOx hydrogen micromix combustion chamber of an industrial gas turbine. *Propulsion and Power research*, 123-131.

Banihabib, R., Lingstadt, T., Wersland, M., Kutne, P., & Assadi, M. (2024). Development and testing of a 100 kW fuel-flexible micro gas turbine running on 100% hydrogen. *International Journal of Hydrogen Energy 49*, 92-111.

Batten, P., Goldberg, U., Kang, E., & Chakravarthy, S. (2011). Smart Sub-Grid-Scale Models for LES and HybridRANS/LES. *Theoretical Fluid Mechanics Conference.* Honolulu: American Institute of Aeronautics and Astronautics.

Beltran, L., Sandoval, J., Llain, J., Carmona, M., & Audivet, C. (2024). Hydrogen combustion in micromix burners: Present stages, opportunities, and challenges. *International Journal of Hydrogen Energy 96*, 622-638.

Benim, A. C. (2024). Investigation into the Computational Analysis of High–Speed Microjet Hydrogen–Air Diffusion Flames. *Fire 7*.

Cappelletti, A., Martelli, F., Bianchi, E., & Trifoni, E. (2014). Numerical redesign of 100kw MGT combustor for 100% H2 fueling. *Energy Procedia 45*, 1412-1421.

Caramia, G., Amirante, R., & De Palma, P. (2024). Unsteady RANS simulations of under-expanded hydrogen jets for internal combustion engines. *International Journal of Hydrogen Energy 96*, 849-859.

Catalano, G., Chang, K. S., & Mathis, J. A. (1989). Investigation of turbulent jet impingement in a confined crossflow. *AIAA*.

Cecere, D., Giacomazzi, E., Di Nardo, A., & Calchetti, G. (2023). Gas turbine combustion technologies for Hydrogen blends. *Energies 16*, 6829.

Charoenchang, W. (2021). *Analysis of Fuel-Air Mixing in Jet in Crossflow.* Gothenburg: Chalmers University of Technology.

Cheng, J., Zong, C., & Zhu, T. (2024). A comparative study of combustion models for simulating partially premixed swirling natural gas flames. *Thermal Science and Engineering Progress 47*.

Corchero, G., & Montañés, J. L. (2005). An approach to the use of hydrogen for commercial aircraft engines. *Journal of Aerospace Engineering 219*, 35-44.

Daurer, G., Schwarz, S., Demuth, M., Gaber, C., & Hochenauer, C. (2024). Evaluation of numerical modeling and combustion characteristics of hydrogen oxy-fuel combustion in a semi-industrial furnace. *Fuel 369*.

Donepudi, T., Pecnik, R., Peeters, J. W., Klein, S., Bouten, T., & Axelsson, L.-U. (2024). Shear-driven Hydrogen-air Mixing in Op16 DLE Combustor: A Comparative Study Between URANS And LES. *Turbomachinery Technical Conference and Exposition.* London: ASME.

Farabi, J., Ismail, M., & Abtahizadeh, E. (2021). Numerical Study of Non-premixed MILD Combustion in DJHC Burner Using Eddy Dissipation Concept and Steady Diffusion Flamelet Approach. *International Journal of Engineering and Manufacturing 3*, 1-17.

Funke, H. H.-W., Beckmann, N., Stefan, L., & Keinz, J. (2023). HYDROGEN COMBUSTOR INTEGRATION STUDY FOR A MEDIUM RANGE AIRCRAFT ENGINE USING THE DRY-LOW NOX “MICROMIX” COMBUSTION PRINCIPLE. *Turbomachinery Technical Conference and Exposition.* Boston: ASME.

Funke, H. H.-W., Boerner, S., Keinz, J., Kusterer, K., Kroniger, D., Kitajima, J., . . . Horikawa, A. (2012). Numerical and Experimental Characterization of Low NOx Micromix Combustion Principle for Industrial Hydrogen Gas Turbine Applications. *Turbine Technical Conference and Exposition* (pp. 1069-1079). Copenhagen: ASME.

Garcia Lovella, Y., Herrera Moya, I., Jayasuriya, J., & Blondeau, J. (2024). Reynolds-average Navier-Stokes turbulence models assessment: A case study of CH4/H2/N2-air reacting jet. *Heliyon 10*.

Gerasimov, A. (2016, May). Quick Guide to Setting Up LES-type Simulations. ANSYS.

Goldmeer, J. (2020). Solving the challenge of lean hydrogen premix combustion with highly reactive fuels. *Turbomachinery International*.

He, D., Yu, Y., Kuang, Y., & Wang, C. (2021). Model Comparisons of Flow and Chemical Kinetic Mechanismsfor Methane–Air Combustion for Engineering Applications. *Applied Sciences 11*.

He, G., Guo, Y., & Hsu, A. T. (1999). The effect of Schmidt number on turbulent scalar mixing. *International Journal of Heat and Mass Transfer 42*, 3727-3738.

Howarth, T. L., Picciani, M. A., Richardson, E. S., Day, M. S., & Aspden, A. J. (2024). Direct numerical simulation of a high-pressure hydrogen micromix combustor: Flame structure and stabilisation mechanism. *Combustion and Flame 265*.

Kazakov, A., & Frenklach, M. (n.d.). *Reduced Reaction Sets based on GRI-Mech 1.2.* Retrieved from http://www.me.berkeley.edu/drm/

Kildare, J. A., Evans, M. J., Tian, Z., & Medwell, P. R. (2024). Estimation and testing of single-step oxidation reactions for hydrogen and methane in low-oxygen, elevated pressure conditions. *Fuel 360*.

Kosiak, P., Yanovych, V., Uruba, V., & Duda, D. (2024). Numerical simulation of the flow topology over NREL's S807 airfoil at different models of turbulence. *EPJ Web of Conferences 299*.

Kumar, N. (2021). *Investigations on NOx emissions from a turbulent non-premixed bluff body stabilized flame.*

Li, J., Zhao, Z., Kazanov, A., & Dryer, F. L. (2004). An Updated Comprehensive Kinetic Model of Hydrogen Combustion. *International Journal of Chemical Kinetics 36*, 566-575.

Long, S., Tian, Z. F., Nathan, G., Chinnici, A., & Dally, B. (2015). CFD Modelling of Isothermal Multiple Jets in a Combustor. *Eleventh International Conference on CFD in the Minerals and Process Industries.* Melbourne: CSIRO.

Madaliev, M., Usmonov, M., Tillaboyeva, F., Mamatov, A., Otakulov, B., Ro'zaliyev, S., & Mamatova, Z. (2024). Comparison of numerical results of RSM turbulence models for the problem of asymmetrical plane diffuser. *BIO Web of Conferences 145*.

Mehl, C., Poncet, S., Truffin, K., & Colin, O. (2024). Large Eddy Simulation of large-scale hydrogen deflagrations using the Thickened Flame Model with stretch sensitivity adaptation and thermo-diffusive instability modeling. *International Journal of Hydrogen Energy 93*, 457-468.

Menter, F. R. (2015). *Best Practice: Scale-Resolving Simulations in.* Ansys.

Mishra, A. A., & Girimaji, S. S. (2017). Toward approximating non-local dynamics in single-point pressure–strain correlation closures. *Journal of Fluid Mechanics 811*, 168-188.

Mueller, M. A., Kim, T. J., Yettter, R. A., & Dryer, F. L. (1999). Flow reactor studies and kinetic modeling of the H2/O2 reaction. *International Journal of Chemical Kinetics 31*, 113-125.

Murugavel, A. B., Massey, J. C., Tanaka, Y., & Swaminathan, N. (2024). The effect of methane addition on reacting hydrogen jets in crossflow. *International Journal of Hydrogen Energy 80*, 57-67.

Nair, V., Sirignano, M., Emerson, B. H., Jiang, N., Felver, J., Roy, S., . . . Lieuwen, T. (2019). Counter rotating vortex pair structure in a reacting jet in crossflow. *Proceedings of the Combustion Institute 37*, 1489-1496.

Nemati, A., Ong, J. C., & Walther, J. H. (2022). CFD analysis of combustion and emission formation using URANS and LES under large two-stroke marine engine-like conditions. *Applied Thermal Engineering 216*.

New, T. H., Lim, T. T., & Luo, S. C. (2006). Effects of jet velocity profiles on a round jet in cross-flow. *Experiments in Fluids 40*, 859–875.

Porcarelli, A., Kruljević, B., & Langella, I. (2023). Suppression of NOx emissions by intensive strain in lean premixed hydrogen flamelets. *International Journal of Hydrogen Energy*, 413-431.

Posch, S., Gößnitzer, C., Lang, M., Novella, R., Steiner, H., & Wimmer, A. (2025). Turbulent combustion modeling for internal combustion engine CFD: A review. *Progress in Energy and Combustion Science 106*.

Praliyev, N., Sarsen, A., Kaishubayeva, N., Zhao, M. Y., Fok, S. C., & Teh, L. S. (2019). A Comparative Analysis of Different Turbulence Models for Simulating Complex Turbulent Separated Flows over Cubic Geometries. *IOP Conference Series Materials Science and Engineering.* Shanghai.

Rahman, M. M. (2023). Capturing transition and non-transition flows with a new shear stress transport model. *Chinese Journal of Aeronautics 36*, 121-136.

Sa, B., Shao, W., Ge, Z., Bi, X., Wang, Z., & Xu, X. (2025). Experimental investigation on macrostructure and evolution of hydrogen-air micro-mix multi-jet flames. *International Journal of Hydrogen Energy 97*, 25-37.

Schiavone, F. G., Detomaso, N., Torresi, M., & Laera, D. (2024). An Arrhenius-based one-step reaction mechanism for hydrogen-air flames simulations in an extended range of operating conditions. *International Journal of Hydrogen Energy 57*, 1229-1243.

Smagorinsky, J. (1963). General circulation experiments with the Primitive Equations. *Monthly Weather Review 91*.

Song, X., Yu, Z., Liu, C., & Cheng, G. (2022). Calibration of RANS model constant based on data assimilation and accurate simulation of separated flow. *AIP Advances 12*.

Speziale, C. G., Sarkar, S., & Gatski, T. B. (1990). *Modeling the Pressure-Strain Correlation of Turbulence - an Invariant Dynamical Systems Approach.* Hampton: Institute for Computer Applications in Science and Engineering, NASA Langley Research Center.

Sternin, A., Ma, H., Liu, J., Haidn, O. J., & Tajmar, M. (2019). *Turbulence, Combustion and Film Prediction in Rocket Application via Parameter Adjustion, Model Variation and Deep Learning Method.*

Sun, W. (2023). Assessment of advanced RANS turbulence models for prediction of complex flows in compressors. *Chinese Journal of Aeronautics 36*, 162-177.

Townsend, J. F., Xu, G., & Jin, Y. (2024). Roughness constant selection for atmospheric boundary layer simulations using a k-ω SST turbulence model within a commercial CFD solver. *Advances in Wind Engineering*.

Vilag, V., Vilag, J., Carlanescu, R., Mangra, A., & Florean, F. (2019). CFD Application for Gas Turbine Combustion Simulations. In *Computational Fluid Dynamics Simulations.*

Wartha, E.-M., Bösenhofer, M., & Harasek, M. (2020). Characteristic Chemical Time Scales for Reactive Flow Modeling. *Combustion Science and Technology*.

Yilmaz, H., Cam, O., Tangoz, S., & Yilmaz, I. (2017). Effect of different turbulence models on combustion and emission characteristics of hydrogen/air flames. *International Journal of Hydrogen Energy 42*, 25744-25755.

Yoder, A., DeBonis, J. R., & Georgiadis, N. J. (2013). *Modeling of Turbulent Free Shear Flows.* Cleveland: Glenn Research Center.

Yoder, D. A., & Orkwis, P. D. (2019). *On the Use of Optimization Techniques for Turbulence Model Calibration.* Cleveland: Glenn Research Center.

Younoussi, S., & Ettaouil, A. (2024). Calibration method of the k-ω SST turbulence model for wind turbine performance prediction near stall condition. *Heliyon 10*.

Yuntao, W., Yulun, Z., Song, L., & Dehong, M. (2015). Calibration of a γ-Reθ transition model and its validation in low-speed flows with high-order numerical method. *Chinese Journal of Aeronautics 28*, 704-711.

Zhang, M., Nie, S., Meng, X., & Zuo, Y. (2022). The Application of the γ-Reθt Transition Model Using Sustaining Turbulence. *Energies 15*.

Zubanov, V. M., Stepanov, D. V., & Shabliy, L. S. (2016). The technique for Simulation of Transient Combustion Processes in the Rocket Engine Operating with Gaseous Fuel “Hydrogen and Oxygen”. *Journal of Physics Conference Series 803*.

Acknowledgements

I wanted to thank everyone who helped me to achieve this important milestone and express my gratitude to all those who supported me in my academic journey.

First, I would like to thank my supervisor Prof. Stefano d'Ambrosio, my company supervisor Dipl. Ing. Alexander Lautenschläger and Dr. Anis Haj Ayed for their guidance and advice during the most stressful of times.

I thank my parents and my siblings for giving me constant motivations to overcome the difficult times and for helping me grow as a student and individual; I take this graduation as an opportunity to show them that their time and effort were not wasted on me, and that I appreciate every time they pulled through to help me in my struggles.

I want to thank my grandparents for their unwavering support and for giving this graduation meaning beyond the accomplishment of the academic feat.

Lastly, I would like to thank all my friends for putting up with me and for setting incredible examples as motivated and accomplished individuals whom I am proud to cherish and support on every occasion.